The Journal of Immunology

Farnesyltransferase Inhibition Exacerbates Eosinophilic Inflammation and Airway Hyperreactivity in Mice with Experimental Asthma: The Complex Roles of Ras GTPase and Farnesylpyrophosphate in Type 2 Allergic Inflammation

Jennifer M. Bratt, Kevin Y. Chang, Michelle Rabowsky, Lisa M. Franzi, Sean P. Ott, Simone Filosto, Tzipora Goldkorn, Muhammad Arif, Jerold A. Last, Nicholas J. Kenyon and Amir A. Zeki

J Immunol 2018; 200:3840-3856; Prepublished online 27 April 2018;
doi: 10.4049/jimmunol.1601317
http://www.jimmunol.org/content/200/11/3840

The Journal of Immunology is published twice each month by
The American Association of Immunologists, Inc.,
1451 Rockville Pike, Suite 650, Rockville, MD 20852

Print ISSN: 0022-1767 Online ISSN: 1550-6606.

Farnesyltransferase Inhibition Exacerbates Eosinophilic Inflammation and Airway Hyperreactivity in Mice with Experimental Asthma: The Complex Roles of Ras GTPase and Farnesylpyrophosphate in Type 2 Allergic Inflammation

Jennifer M. Bratt,*,† Kevin Y. Chang,* Michelle Rabowsky,* Lisa M. Franzi,*,† Sean P. Ott,*,† Simone Filosto,*,†,‡ Tzipora Goldkorn,*,†,‡ Muhammad Arif,*,† Jerold A. Last,*,† Nicholas J. Kenyon,*,† and Amir A. Zeki*,†

Ras, a small GTPase protein, is thought to mediate Th2-dependent eosinophilic inflammation in asthma. Ras requires cell membrane association for its biological activity, and this requires the posttranslational modification of Ras with an isoprenyl group by farnesyltransferase (FTase) or geranylgeranyltransferase (GGTase). We hypothesized that inhibition of FTase using FTase inhibitor (FTI)–277 would attenuate allergic asthma by depleting membrane-associated Ras. We used the OVA mouse model of allergic inflammation and human airway epithelial (HBE1) cells to determine the role of FTase in inflammatory cell recruitment. BALB/c mice were first sensitized then exposed to 1% OVA aerosol or filtered air, and half were injected daily with FTI-277 (20 mg/kg per day). Treatment of mice with FTI-277 had no significant effect on lung membrane–anchored Ras, Ras protein levels, or Ras GTPase activity. In OVA-exposed mice, FTI-277 treatment increased eosinophilic inflammation, goblet cell hyperplasia, and airway hyperreactivity. Human bronchial epithelial (HBE1) cells were pretreated with 5, 10, or 20 μM FTI-277 prior to and during 12 h IL-13 (20 ng/ml) stimulation. In HBE1 cells, FTase inhibition with FTI-277 had no significant effect on IL-13–induced STAT6 phosphorylation, eotaxin-3 peptide secretion, or Ras translocation. However, addition of exogenous FPP unexpectedly augmented IL-13–induced STAT6 phosphorylation and eotaxin-3 secretion from HBE1 cells without affecting Ras translocation. Pharmacological inhibition of FTase exacerbates allergic asthma, suggesting a protective role for FTase or possibly Ras farnesylation. FPP synergistically augments epithelial eotaxin-3 secretion, indicating a novel Ras-independent farnesylation mechanism or direct FPP effect that promotes epithelial eotaxin-3 production in allergic asthma. ***The Journal of Immunology*****, 2018, 200: 3840–3856.**

Asthma is a chronic allergic disease affecting 300 million adults and children worldwide (1). Although conventional treatments, such as inhaled corticosteroids (ICS), can reduce exacerbation rates in patients with mild or moderate asthma, they do not alter the course of the disease and have limited efficacy in some severe asthma patients. A better understanding of asthma pathogenesis can lead to novel therapies that better target specific subpopulations of asthmatics who do not respond to conventional therapies.

The mevalonate (MA) metabolic cascade is a ubiquitous anabolic biochemical pathway essential for cellular function in both prokaryotic and eukaryotic organisms. MA is the immediate product of HMG-CoA reductase (HMGCR), the rate-limiting step in cholesterol biosynthesis in the MA pathway (Fig. 1). MA is further metabolized into the lipid isoprenoid intermediates farnesylpyrophosphate (FPP) and geranylgeranylpyrophosphate (GGPP), in which FPP can also convert to GGPP or squalene, an important lipid precursor of cholesterol (2) (Fig. 1).

HMGCR inhibitors (also known as statins) inhibit the synthesis of the isoprenoids and cholesterol by directly inhibiting HMGCR, which depletes the pool of available MA. We and others showed that statins reduce murine allergic airway inflammation, attenuate airway hyperreactivity (AHR), and inhibit early hallmarks of airway remodeling (3–5), such as goblet cell hyperplasia and arginase protein expression and enzyme activity (6, 7). Although we recognize the pleiotropic effects of statins and their potential off-target effects (8–10), the anti-inflammatory statin effects in the OVA mouse model and in human airway epithelial cells appear to occur primarily via inhibition of HMGCR (6, 7, 11).

The prenyltransferases, including farnesyltransferase (FTase) and geranylgeranyltransferase (GGTase-I/II), catalyze the attachment of

*Division of Pulmonary, Critical Care, and Sleep Medicine, Department of Internal Medicine, University of California, Davis, Davis, CA 95817; †Department of Internal Medicine, Center for Comparative Respiratory Biology and Medicine, University of California, Davis, Davis, CA 95817; and ‡Department of Internal Medicine, Respiratory Signal Transduction, Genome and Biomedical Sciences Facility, University of California, Davis, Davis, CA 95616

ORCIDs: 0000-0001-9660-5634 (J.M.B.); 0000-0001-7477-5763 (K.Y.C.); 0000-0003-4181-277X (L.M.F.); 0000-0001-8792-7236 (S.P.O.).

Received for publication July 29, 2016. Accepted for publication March 14, 2018.

This work was supported by National Institutes of Health Grant T32 HL07013 (to J.M.B. and A.A.Z.), National Center for Advancing Translational Sciences Grant UL1 TR000002 (to A.A.Z.), National Heart, Lung, and Blood Institute Grant HL105573 (to N.J.K.), the Northern California Health Care System Medical Center Department of Veterans Affairs, an American Thoracic Society Fellows Career Development Award (to A.A.Z.), National Institutes of Health Grants KL2 RR 024144 (to A.A.Z.), 1K08HL114882-01A1 (to A.A.Z.), and R01-HL-66189 (to T.G.), Tobacco-Related Disease Research Program Grant TRDRP-0087 (to S.F.), and National Institute for Occupational Safety and Health Grant U54 OH007550 (to J.A.L.).

Address correspondence and reprint requests to Prof. Amir A. Zeki, University of California, Davis, Genome and Biomedical Sciences Facility, 451 Health Sciences Drive, Room 6517, Davis, CA 95616. E-mail address: aazeki@ucdavis.edu

Abbreviations used in this article: ACM, alveolar-capillary membrane; AHR, airway hyperreactivity; BALF, bronchoalveolar lavage fluid; BP, bisphosphonate; Cdyn, dynamic compliance; FA, filtered air; FPP, farnesylpyrophosphate; FPPS, FPP synthase; FTase, farnesyltransferase; FTI, FTase inhibitor; GGPP, geranylgeranylpyrophosphate; GGTase, geranylgeranyltransferase; GR, glucocorticoid receptor; HMGCR, HMG-CoA reductase; ICS, inhaled corticosteroid; IPP, isopentenyl pyrophosphate; MA, mevalonate; MCh, methacholine; PAS, periodic acid–Schiff; Rrs, respiratory system resistance.

farnesyl or geranylgeranyl groups to Ras and Rho/Rab family GTPases, respectively, a reaction collectively known as isoprenylation (12) (Fig. 1). The FTase enzyme recognizes FPP and also binds the CaaX box motif located on the C terminus of proteins, such as Ras GTPase, catalyzing the formation of the thioester linkage between the cysteine of the CaaX motif and the C1 of the FPP molecule (13). These are critical posttranslational protein modifications that allow Ras GTPases to anchor in cell membranes to affect signal transduction (14).

Although statins deplete MA and downstream FPP and GGPP to *indirectly* reduce farnesylation and geranylgeranylation events, the FTase inhibitors (FTI) and GGTase inhibitors *directly* block farnesylation and geranylgeranylation, respectively (2, 13). Therefore, it is important to determine which subarm of the MA pathway (the isoprenoid [FTase/Ras family, GGTase-I/Rho family, and GGTase-II/Rab] or sterol [squalene/cholesterol] parts) mimics the beneficial statin effect observed in asthma.

RhoA activity is elevated in allergic asthma (15–17), and GGTase-I inhibition mitigates eosinophilic inflammation and AHR in a murine model of allergic inflammation (16–18). Our study focuses on the FTase enzyme (Fig. 1) because it promotes Ras GTPase signaling in cells, a process thought to be necessary for eosinophilic inflammation and the development of Th2/type 2 allergic asthma (19–22).

In animal models of allergic asthma, Ras modulates T cell–dependent allergic inflammation and eosinophilic trafficking and transmigration (19, 21–23). Previous work by Myou et al. (19) using dominant–negative Ras constructs to nullify Ras activity showed that Ras was necessary for this Th2 induction in mice. However, despite the apparent role of Ras in allergic inflammation, no one has investigated the contributions of FTase to asthma pathogenesis. To further understand the mechanism of the statin-dependent anti-inflammatory effect in asthma (6, 24, 25), we investigated the role of Ras protein farnesylation via the actions of FTase in normal and inflamed murine lungs and in human airway epithelial cells.

In this study, we hypothesized that pharmacological inhibition of FTase activity would 1) reduce Ras membrane association, 2) reduce overall Ras GTPase activity, and 3) inhibit indicators of allergic type 2 inflammation (eosinophilic airway inflammation, lung STAT6 activation, goblet cell metaplasia or hyperplasia, and AHR). To test this hypothesis, we investigated the therapeutic potential of FTI-277 in vivo using the OVA mouse model and examined its effect on Ras membrane localization and enzyme activity in lung tissues. We then examined the effect of FTI-277 on IL-13–dependent STAT6 activation and eotaxin-3 (CCL26) production in vitro using HBE1 human bronchial epithelial cells to examine the mechanism in a single-cell type relevant to type 2 (Th2) asthma. Downstream of the IL-13R, a key Th2 effector molecule in asthma, STAT6 is the primary transcription factor for eotaxin-1, -2, and -3 gene expression. Eotaxin-3 has clinical relevance in IL-13–mediated inflammation and human severe asthma (26, 27) and is one of the main chemokines associated with Th2-high inflammation and airway eosinophilia in asthma (26)

To our surprise, the results of these experiments unexpectedly supported the null hypothesis that systemic treatment of allergic mice with FTI-277 further exacerbated eosinophilic airway inflammation, worsened AHR, and increased goblet cell hyperplasia. These results further compelled us to conduct in vitro cell culture experiments, which allowed us to isolate drug effects in a single-cell type to better understand our in vivo results. Our cell culture experiments were necessary for three reasons: 1) given the complexity of Ras and FTase biology in the intact animal host (assayed as whole-lung homogenates), results of FTase antagonism in vivo can be difficult to interpret when using pharmacologic inhibition alone; 2) evaluating Ras and FTase mechanisms in HBE1 cells is important given that the airway epithelium plays a central role in human asthma pathogenesis (i.e., elucidating the contribution of epithelial FTase inhibition to allergic inflammation); and 3) understanding drug effects on airway epithelial cells has direct implications for the development of inhaler therapies.

Although treatment with FTI-277 inhibited Ras farnesylation and therefore depleted membrane-anchored Ras in HBE1 cells at shorter treatment durations (i.e., 30 min), treatment of HBE1 cells with FTI-277 for longer durations (i.e., 72 h) had no significant effect on Ras membrane/cytosol translocation, IL-13–induced STAT6 activation, or eotaxin-3 peptide secretion. Interestingly, exogenous treatment of HBE1 cells with the isoprenoid FPP further augmented IL-13–induced STAT6 phosphorylation and eotaxin-3 secretion beyond the activating effects of IL-13 alone.

Our findings provide further evidence that the MA cascade plays an important role in asthma pathogenesis and contributes to our understanding of the interrelated roles of Ras, FTase, and FPP in allergic inflammation. Our data suggest that FTase and Ras GTPase have complex and possibly protective roles in normal physiology and asthma pathogenesis. FPP itself markedly increases eotaxin-3 production in human airway epithelial cells, an unexpected finding worthy of further study. Excess airway FPPs from cellular sources may play a role in perpetuating eosinophilic airway inflammation in asthma.

Materials and Methods

Drug inhibitor

FTI-277 and FPP were purchased from Sigma-Aldrich (St. Louis, MO). FTI-277 is a Ras CaaX peptidomimetic (Fig. 1) with an IC_{50} of 50 nM (Sigma-Aldrich). FTI-277 was dissolved in DMSO at a concentration of 10 mM and stored at −20°C for future application. The 10 mM FTI-277 solution was further diluted using sterile PBS at pH 7.4 for all experiments. For in vivo experiments, the FTI-277 final concentration was 2.5 mg/ml (equivalent to a dosage of 20 mg/kg or 0.5 mg/mouse per day). FPP was initially dissolved in a solution of methanol and 10 mM ammonium hydroxide (NH_4OH) to a concentration of 1 μg/μl and stored at −20°C. FPP was further diluted to the desired concentrations (5, 10, and 20 μM) in sterile PBS for use in cell culture experiments. The vehicle control for FPP was its chemical solvent methanol/NH_4OH (70:30). Previous experiments in our laboratory showed no evidence of cytotoxicity of this solvent in HBE1 cells using either MTT or Alamar blue assays.

Animals

Eight-week-old pathogen-free male BALB/c mice were purchased from Charles River Laboratories (Wilmington, MA). Mice were housed and cared for by the veterinary staff of the University Laboratory Animal Resources at the University of California, Davis, following institutional standards and regulations for animal care and use. All mice were maintained in a high efficiency particulate air–filtered laminar flow cage rack with a 12 h light/dark cycle with free access to water and food throughout the study and were routinely screened for health status. All procedures were performed following our Institutional Animal Care and Use Committee–approved protocol. Animal weights were measured prior to allergen sensitization and on days 1, 3, and 6 post FTI-277 injections.

Drug regimen and OVA aerosol exposures

Mice were sensitized by two i.p. injections of 10/0.1 μg/ml OVA in PBS (pH 7.4) with alum adjuvant on day 0 and 14. After sensitization, mice were divided into four treatment groups as follows: OVA plus PBS ($n = 6$), OVA plus FTI-277 ($n = 6$), filtered air (FA) plus PBS ($n = 4$), and FA plus FTI-277 ($n = 4$).

Starting on day 28, mice received daily i.p. injections of 20 mg/kg FTI-227 (equivalent to 0.5 mg per mouse per day), administered 30 min prior to OVA/FA exposures for 14 d during the 2-wk OVA exposure period. OVA aerosol exposures began on day 28 and were performed using nebulizers and aerosol exposure chambers as described previously (28, 29). Briefly, OVA treatment groups were exposed to aerosol derived from 10 ml of 1% (w/v) OVA in PBS (for 30 min), three times a week over a duration of 2 wk and

for a total of six exposures (i.e., 6OVA). Aerosol delivery was performed using a side-stream nebulizer (Invacare, Elyria, OH) and air compressor (Invacare, Sanford, FL). Aerosol characterization was performed as described in Kenyon et al. (30).

Lung physiology measurements

Pulmonary function parameters were measured using a Buxco restrained whole-body plethysmograph (Buxco Electronics, Troy, NY). After the final OVA aerosol or FA exposure, mice were anesthetized and sedated using a dose of 0.5 mg/kg medetomidine (Dormitor; Orion Pharma, Espoo, Finland) and tiletamine-zolazepam (Telazol; Fort Dodge Laboratories, Fort Dodge, IA). The mice were then cannulated with a blunt-tipped tube for mechanical ventilation (MiniVent; Harvard Apparatus, Cambridge, MA) at a stroke volume of 200 μl and a frequency of 150 breaths/min.

Lung dynamic compliance (Cdyn, ml/cm H_2O) and total respiratory system resistance (Rrs, cm H_2O s/ml) were calculated at baseline, using 3 min average values, and over a course of nebulized aerosols of saline and methacholine (MCh) dose response challenge (0, 0.5, 1.0, and 2.0 mg/ml), as described in detail previously by Zeki et al. (6).

Tissue processing and bronchoalveolar lavage fluid inflammatory cell counts

Immediately after collection of lung physiology measurements, mice were sacrificed with an overdose of Beuthanasia-D (pentobarbital sodium and phenytoin sodium). Lungs were lavaged twice with 1 ml of PBS (pH 7.4) containing 1 mM PMSF and 1:100 v/v protease inhibitor mixture (Sigma-Aldrich) and centrifuged at 325 × *g*. Bronchoalveolar lavage fluid (BALF) supernatant was decanted and stored at −20°C for multiplex cytokine profiling and albumin measurements. The cell pellet was resuspended in ACK lysis buffer (0.15 M NH_4Cl, 1 mM $KHCO_3$, 0.1 mM EDTA [pH 7.3]) to lyse RBCs then centrifuged and resuspended in 0.5 ml PBS. The total live cell number from lavage was determined by Trypan Blue Exclusion using a standard manual hemacytometer.

Single 100-μl aliquots from each of the cell suspensions were processed onto slides using a cytocentrifuge at 1650 rpm for 7 min. Slides were stained with a Hema 3 Stain set per the manufacturer's instructions (Thermo Fisher Scientific, Kalamazoo, MI). BALF cell percent differentials were determined by counting 10 fields under a 40× objective, based on morphological characteristics and staining profiles.

After lung lavage, the right bronchus of each lung was ligated using surgical suture. The right bronchus was severed distal to the ligation suture and snap frozen at −80°C for future use. The remaining left lung was fixed in situ for histological evaluation at 20 cm H_2O with 1% paraformaldehyde (in PBS at pH 7.4) and processed for paraffin embedding as described in Zeki et al. (7).

Mouse lung tissue homogenization and fractionation

Lung homogenates were prepared from the right superior and middle lung lobes using isolation buffer (250 mM sucrose, 20 mM HEPES [pH 7.4], 2 mM EDTA, and 3 mM NaN_3) containing protease inhibitors (Protease Inhibitor [1:100; Sigma-Aldrich], 1 mM PMSF, 1 mM Na_3VO_4, and 1 mM NaF) and Phosphatase Inhibitor (1:100; Sigma-Aldrich). The lung tissue was homogenized by hand using a chilled Dounce homogenizer. The resulting crude homogenates were centrifuged at 800 × *g* for 5 min at 4°C. The supernatant was removed, and total protein concentration was determined using the BCA Protein Assay (Pierce Biotechnology, Rockford, IL).

Homogenates were diluted to 5 μg/μl, and an aliquot was reserved as the total homogenate. A 200-μl aliquot of total homogenate was ultracentrifuged at 30,000 × *g* at 4°C for an additional 30 min to separate the cytosolic and membrane components. The supernatant from this step was collected (~200 μl) and referred to as the cytosolic fraction. The remaining pellet was resuspended in 200 μl isolation buffer and referred to as the membrane fraction. All subcellular fractions were stored at −80°C.

Western blot analyses

SDS-PAGE electrophoresis was performed on the cytosolic and membrane fractions (30 μg total protein) under reducing conditions and transferred to a PVDF membrane. The gel composition differed slightly for Ras as compared with other proteins, in which a 12% gel was used for Ras and 10% for all other proteins. This facilitated better protein separation for Ras isoforms and the assessment of farnesylated versus unfarnesylated Ras. Membranes were probed using rabbit (anti-mouse) anti-Ras IgG (1:1000, 100 μl; Cell Signaling Technology), monoclonal anti–E-cadherin IgG (1:1000, 0.1 μg/ml; BD Biosciences, San Jose, CA), anti-GAPDH IgG_1 (1:50,000, 200 μg/ml; Santa Cruz Biotechnology, Dallas, TX), rabbit anti–α-actinin IgG (1:1000; Santa Cruz Biotechnology), and rabbit total- and phospho-STAT6 IgG (primary Ab 1:1000, secondary Ab goat anti-rabbit 1:10,000) at 4°C followed by incubation in 40 ng/ml HRP-conjugated goat anti-rabbit IgG (Pierce Biotechnology) or HRP-conjugated goat anti-mouse IgG (R&D Systems, Minneapolis, MN) in 5% dry milk in 0.05% Tween 20 in PBS. Bands were visualized using Western Lightning Plus-ECL substrate (PerkinElmer, Shelton, CT) and Image Reader LAS-4000 V2.1 (Fujifilm, Cypress, CA) or the Konica SRX 101A Medical Film Processor. Films were scanned using a Canon ImageRunner 3235 scanner. Band intensity was calculated using ImageJ (National Institutes of Health Freeware).

E-cadherin, unique to cell plasma membranes, was used as a marker of reliable separation between membrane and cytosolic fractions. GAPDH or α-actinin were used as protein loading controls for the cytosolic fraction when appropriate. E-cadherin separations equivalent to membrane fractions >95% and cytosolic fractions <5% confirmed consistent subcellular fraction separation across all treatment groups (and vice versa for GAPDH when >95% was in the cytosolic fraction).

Ras activation assay

Cytoskeleton Precision Red Advanced Protein Assay Reagent was used to determine total protein concentration in each of our samples. Ras GTPase activity was measured in the membrane and cytosolic fractions using the Ras Activity ELISA ASSAY Kit (EMD Millipore, Billerica, MA), which uses an rRaf-1-RBD to bind active Ras. The assay was performed per the manufacturer's instructions using 20 μg/μl total protein concentration. Active Ras was measured using the Packard LumiCount Luminometer Plate Reader version 3.0 at λ = 600 nm (PerkinElmer, Waltham, MA).

BALF cytokine and chemokine assay

Cytokine screening for selected Th1 and Th2 cytokines and chemokines from BALF supernatant was performed using MILLIPLEX MAP Mouse Cytokine/Chemokine Magnetic Bead Panel (EMD Millipore, St. Charles, MO). The cytokine panel included IL-13, IL-4, IL-5, eotaxin, IL-10, IL-1α, IL-1β, IL-2, IP-10, IL-12, MCP-1, IL-9, VEGF, KC, G-CSF, LIX, MIP-1α, MIP-1β, MIG, LIF, M-CSF, RANTES, IL-17, IL-3, IL-7, IL-12, IL-15, GM-CSF, IFN-γ, IL-6, MIP-2, and TNF-α. For cytokine and chemokine sample measurements below the detection limit, results were assigned a value equal to the minimal detection limit for the specific assay to facilitate statistical analysis.

Histological analyses

Paraffin-embedded left lung lobes were sectioned at 5 μm parallel to the major conducting airways. Tissue sections were selected for staining by visual evaluation of airway branching to maximize the representation of conducting airways. H&E staining and periodic acid–Schiff (PAS) staining were performed on sections from two to three animals per group as described in Zeki et al. (7).

H&E-stained lung sections were scored by two treatment-blinded investigators. Peribronchial and perivascular inflammation were evaluated based upon a subjective scale of 0–5. Each slide was reviewed randomly and scored independently by at least two investigators. Scores were based on the following scale: 0 = no detectable inflammation, 2.5 = moderate inflammation with a layer of inflammatory cells encircling the bronchi and peribronchioles approximately three cells deep, and 5 = extensive inflammation with a layer of inflammatory cells encircling bronchi and bronchioles >5 cells deep. Scores were averaged for each animal, denoting the inflammation grade as seen in Fig. 4D.

PAS-stained sections were scored as follows: from each lung section, five regions were evaluated, consisting of two segments of primary conducting airway, two secondary conducting airways, and one tertiary conducting airway. A minimum of 100 sequential airway cells were counted from each region, and the total number of PAS-positive cells per total airway was determined. The regional values were averaged to give a final PAS score per animal termed %PAS (+) Epithelial Cells, as seen in Fig. 6B.

Albumin assay

The amount of albumin present in the supernatant of our BALF was measured using a Mouse Albumin ELISA kit (GenWay Biotech). The BALF supernatant was diluted to a concentration of 1:80,000 using the diluent provided in the kit. The protocol provided in the kit was followed per the manufacturer's instructions. The assay was read using the EMax Endpoint ELISA Microplate Reader from Molecular Devices, set at a wavelength of 450 nm. Data are represented as OD.

Cell culture

HBE1 cells are an immortalized human bronchial epithelial cell line (31–35). HBE1 cells (passage 18) were grown to at least 90% confluence on a 100-mm cell culture plate in serum-free medium containing Ham's

F12/DMEM (1:1), 15 mM $NaHCO_3$, 15 mM HEPES (pH 7.4), with the following six factors: transferrin (5 μg/ml), insulin (5 μg/ml), cholera toxin (10 ng/ml), epidermal growth factor (10 ng/ml), dexamethasone (0.1 μM), and bovine hypothalamus extract (15 μg/ml), then transferred to six-well plates under submerged-media conditions. All treatments were performed in triplicate in at least three independent experiments to verify findings.

Experiment no. 1 (n = 3). For examination of FTI-277 effects on Ras translocation between cytosol and membrane, HBE1 cells grown to ≥90% confluence were treated with DMSO drug vehicle, 10 μM FTI-277, and 20 μM FTI-277 for 30 min. After FTI treatment, the medium was removed, and adherent cells were homogenized and processed by ultra-centrifugation into cytosolic and membrane fractions.

Experiment no. 2 (n = 3). HBE1 cells grown to ≥90% confluence were pretreated with FTI-277 (20 μM), FPP (10 μM), FTI plus FPP, or vehicle control for 60 h followed by 12 h costimulation with IL-13 (20 ng/ml) (total of 72 h drug treatment duration). Additional experiments using lower FTI-277 doses at 5 and 10 μM were also conducted. Cell-free media were collected for eotaxin-3 ELISA measurements, and adherent cells were treated with radioimmunoprecipitation assay buffer (catalog no. 89900, ThermoFisher) containing a Protease Inhibitor mixture (1:100; Sigma-Aldrich), PMSF (1 mM; Sigma-Aldrich), and Phosphatase Inhibitor (1:100; Sigma-Aldrich) for isolation of protein from cell homogenates. Media was ultracentrifuged at 10,000 rpm at 4°C for 10 min, and then cell-free culture medium supernatant was collected and stored at −80°C.

We used standard brightfield light microscopy and the Alamar blue assay to assess cell morphology, viability, and mitochondrial function. We did not detect any adverse or cytotoxic effects of FTI-277, FPP, or their respective vehicles (DMSO or methanol/NH_4OH) alone or in combinations at the doses and treatment durations used in all of our experiments.

Epithelial cell tissue homogenization and fractionation

Cells from Experiment no. 1 were scraped and suspended in isolation buffer (250 mM sucrose, 20 mM HEPES, pH 7.4, 2 mM EDTA, and 3 mM NaN_3) containing protease inhibitors (Protease Inhibitor [1:100; Sigma], 1 mM PMSF, 1 mM Na_3VO_4, and 1 mM NaF) and Phosphatase Inhibitor (1:100; Sigma-Aldrich). Further homogenization was performed by hand using a prechilled Dounce homogenizer. The resulting crude homogenates were centrifuged at 800 × *g* for 5 min at 4°C. The supernatant was removed and reserved as the total homogenate. An aliquot of this total homogenate was ultracentrifuged again at 17,500 rpm (~30,000 × *g*) at 4°C for an additional 30 min to separate the cytosolic and membrane components. The supernatant from this step was collected and referred to as the cytosolic fraction. The remaining pellet was resuspended in the same volume of isolation buffer and considered the membrane fraction.

Like our mouse specimens, proper subcellular fractionation was confirmed by assessing for a membrane-only constituent protein (E-cadherin) and a cytosol-only constituent protein (GAPDH). These proteins were used as markers of reliable separation between membrane and cytosolic fractions. E-cadherin separation equivalent to membrane fraction >95% and cytosolic fraction <5% confirmed consistent and successful separation of subcellular fractions across all treatment groups.

The total protein concentration of the cytosolic fraction from each sample was measured using the Micro BCA Protein Assay Kit (Pierce Biotechnology) and used to determine protein loading volumes for each sample.

Eotaxin-3 ELISA

Eotaxin-3 peptide concentration in HBE1 cell media was determined in the cell-free supernatant. Eotaxin-3 peptide concentrations (picograms per milliliter) were determined using the DuoSet ELISA kit, performed according to the manufacturer's instructions (R&D Systems) and per our standard ELISA laboratory techniques.

Statistical analysis

Data were analyzed using the Prism 5 software package (GraphPad Software, San Diego, CA). Raw data were assessed for normality using D'Agostino and Pearson omnibus test, and then tested for statistical significance using parametric or nonparametric tests when appropriate. Values greater than two SD outside the mean were not included in relevant analyses. Parametric data were analyzed using *t* test, one-way ANOVA with Tukey posttest correction, or two-way ANOVA with Bonferroni posttest correction. Nonparametric data were analyzed using the Mann–Whitney or Kruskal–Wallis test with Dunn's posttest correction. When necessary, some data were log transformed prior to statistical analysis. Data are plotted as mean ± SEM except where indicated. A two-tailed α was used in all analyses, and a p value < 0.05 was considered statistically significant.

Results

Blockade of Ras farnesylation through FTase inhibition with FTI-277 shifts subcellular localization of Ras from the membrane to the cytosol (36, 37) and results in loss of Ras-signaling activity (Fig. 1). Therefore, we designed experiments using both mice and HBE1 human bronchial epithelial cells to measure Ras protein levels in the membrane and cytosol of mouse whole-lung and cultured HBE1 cell homogenates. To assess FTI-277 effects on Ras-GTPase function, we also measured Ras enzyme activity in those same subcellular fractions as Ras protein expression in mouse lungs, and correlated our findings to indices of inflammation, airway epithelial remodeling, and lung physiology.

We used FTI-277 in the same in vivo mouse model of allergic airway inflammation used in our previously published simvastatin experiments to compare the effects of FTI-277 on the same indicators of allergic airway inflammation. Mice were treated daily for 14 d with i.p. injections of FTI-277 in combination with OVA aerosol or FA exposure to assess changes in Ras protein and enzymatic activity in mouse whole-lung tissue, in addition to the classic hallmarks of asthma pathology.

Ras subcellular localization in mouse lungs

In FA mice, total Ras protein present in the membrane fraction was greater than Ras in the cytosolic fraction (Fig. 2A). In contrast, mice exposed to OVA aerosol showed no significant difference in Ras protein levels between the membrane and cytosolic fractions, indicating a relative increase in Ras cytosolic fraction relative to membrane fraction (Fig. 2). In both exposure groups, FA and OVA, treatment with FTI-277 had no significant effect on either total Ras protein expression (Fig. 2B) or Ras cytosolic and membrane distribution in whole-lung tissue homogenate (Fig. 2A, 2C, 2D). In Fig. 2A, all cytosolic bands represent unfarnesylated Ras, including the faint band above the lowest one (dashed black arrow), and the membrane bands represent farnesylated membrane–anchored Ras (solid black arrows).

In the OVA groups in Fig. 2D, we observed that there was a relative increase in the Ras cytosolic fraction relative to membrane fraction. It is not clear whether this is a result of membrane–cytosol Ras translocation or of an increase in cytosolic Ras due to the influx of inflammatory cells, such as eosinophils. These data indicate that although OVA exposure alters the relative ratio of cytosolic to membrane-associated Ras, treatment with FTI-277 does not alter Ras translocation between cell membrane and cytosol in mouse whole-lung homogenate at the dose and the time evaluated.

Ras GTPase enzyme activity in mouse lungs

In addition to assessing changes in subcellular localization of Ras protein, we also measured Ras GTPase enzymatic activity in both the unfractionated total homogenate and the cytoplasmic and membrane subcellular fractions.

In the unfractionated homogenates, when animals were combined by exposure type (OVA versus FA) Ras GTPase activity in the OVA group was 2.61-fold higher than FA-exposed control mice (**$p = 0.0022$, by *t* test; Fig. 3A). Treatment with FTI-277 had no measurable effect on total Ras GTPase activity in either the OVA or FA groups compared with their corresponding vehicle controls (Fig. 3B). However, as compared with Fig. 3A, OVA exposure resulted in higher Ras GTPase activity as compared with FA controls in the FTI-treated mice (Fig. 3B, *$p < 0.05$ by one-way ANOVA). This indicates that OVA exposure is associated with increased Ras GTPase activity likely secondary to increased lung inflammation.

Using the fractionated samples, we compared Ras GTPase activity in the cytosolic and membrane fractionated lung samples.

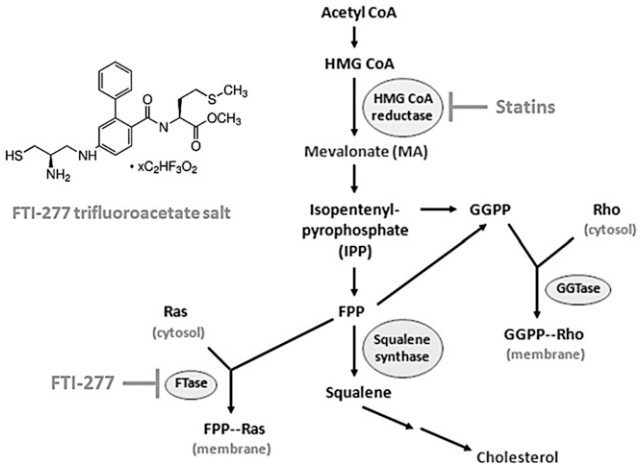

FIGURE 1. The MA pathway. Previous work has established that inhibition of HMGCR with a statin drug significantly reduces eosinophilic airway inflammation and AHR in experimental allergic asthma. To further elucidate the role of the FTase arm of the MA pathway in mediating type 2/Th2 inflammation, we used FTI-277 to inhibit FTase enzyme activity. GGTase and squalene synthase are the alternate arms of the MA pathway but were not assessed in this study. The chemical structure of FTI-277 (a Ras CaaX motif peptidomimetic) is shown in the inset.

FA-exposed mice had significantly greater Ras GTPase activity in the membrane fraction as compared with the cytosolic fraction (***$p < 0.001$ by one-way ANOVA, Fig. 3C), corresponding to Ras subcellular distribution in Fig. 2A. OVA-exposed mice had no statistically significant differences in Ras GTPase activity between the two fractions (Fig. 3C), also consistent with the Ras subcellular distribution shown in Fig. 2D. The pattern of relative Ras protein expression in the different subcellular compartments (Fig. 2D) appears to correlate with the pattern of Ras GTPase activity (Fig. 3D), indicating that Ras enzyme activity likely reflects Ras protein levels in vivo in whole-lung specimens. These data indicate that at baseline in naive noninflamed mice, Ras GTPase is predominantly membrane bound (Fig. 2) and enzymatically active (Fig. 3). And under OVA-induced inflammation, Ras GTPase has increased enzymatic activity in both the cytosolic and membrane fractions as compared with FA control mice (Fig. 3C).

When samples are separated by exposure group and FTI treatment, only the FA plus PBS group had a statistically significant difference in Ras GTPase activity between the cytosol and membrane fractions (Fig. 3D). Treatment with FTI-277 had no statistically significant effect on Ras GTPase activity in either the OVA or FA groups (Fig. 3D). In addition, there was a near equalization in Ras GTPase activity between the cytosolic and membrane fractions in both OVA treatment groups (Fig. 3D). This means that during OVA-induced inflammation there is a significant amount of Ras GTPase activity in the cytosol, unlike their respective FA controls. This finding suggests that cytosolic Ras can be active under certain conditions of inflammation, contrary to current dogma.

We did not further investigate whether this increase in cytosolic Ras activity was due to a change in Ras translocation inside resident lung cells or the effect of increased cytosolic Ras activity in influxed lung inflammatory cells. Ras GTPase activity has a strong positive linear correlation with BALF total cell count and BALF absolute eosinophil count (Fig. 3E), suggesting the increase in Ras activity may be driven by airway or lung eosinophilia.

Allergic airway inflammation

The Ras GTPase/ERK pathway drives the IL-5–dependent effects on cellular proliferation and survival (22, 38), which may augment eosinophilic inflammation. Biochemically, this requires the proper

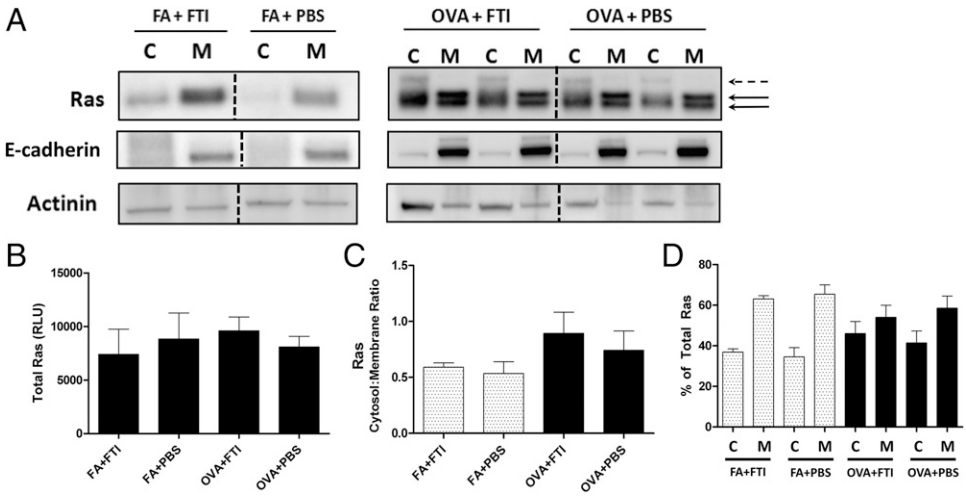

FIGURE 2. Subcellular localization of Ras in air- and allergen-exposed mice and the effects of FTI-277 treatment on Ras subcellular translocation. BALB/c mice were sensitized to OVA and then challenged with 1% OVA aerosol or FA air six times over a 2 wk period. Mice were injected daily with FTI-277 (20 mg/kg per day, i.p.) before each OVA aerosol exposure. Whole-lung homogenates were processed into cytosolic and membrane subcellular fractions, and Ras protein expression in these fractions was assessed by Western blot. Ras semiquantitative values were normalized using E-cadherin and actinin for membrane and cytosolic fractions, respectively. (**A**) In mice exposed to FA, Ras resides predominantly in the membrane fraction. With OVA exposure, Ras becomes nearly evenly distributed between the cytosolic and membrane fractions. These data indicated that under basal noninflamed conditions, Ras is farnesylated and membrane bound. All cytosolic bands represent unfarnesylated Ras, including the faint band above the lowest one (dashed black arrow), and the membrane bands represent farnesylated membrane-anchored Ras (solid black arrows). The dashed black vertical lines represent the space where images of bands were joined from a single blot to show the representative bands shown here. All relevant bands (and blots), including the representative bands above, were used to generate and analyze the data shown in (**B**)–(**D**). (B) Total Ras protein expression did not differ with FTI-277 treatment for both the FA and OVA groups (p = NS by one-way ANOVA). (C) Plotted as cytosol/membrane ratio, treatment with FTI-277 did not affect Ras translocation in both FA and OVA groups (p = NS by one-way ANOVA). (D) Plotted as percentage of total Ras, treatment with FTI-277 showed no statistically significant changes in cytosolic- or membrane-associated Ras in both FA and OVA groups (p = NS by one-way ANOVA). Similarly, there were no significant changes in cytosolic or membrane subcellular fractions in PBS controls for both FA and OVA groups (p = NS by one-way ANOVA).

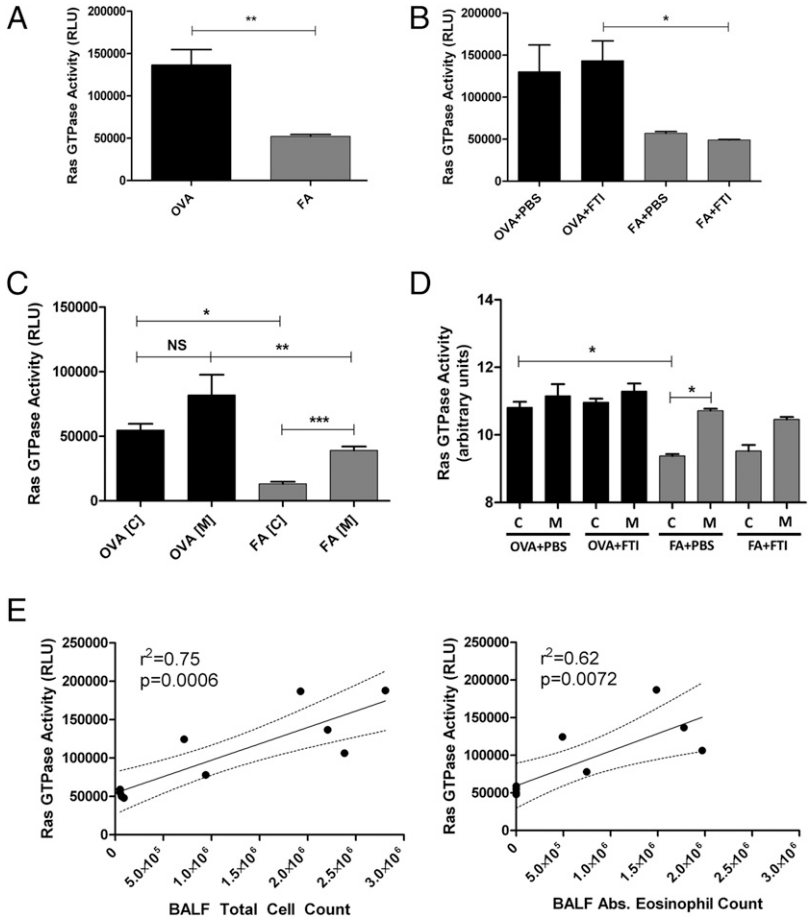

FIGURE 3. Effect of FTI-277 treatment on Ras GTPase activity in mouse lung. BALB/c mice were sensitized to OVA and then challenged with 1% OVA aerosol or FA six times over a 2 wk period. Mice were injected daily with FTI-277 (20 mg/kg per day, i.p.) before each OVA aerosol exposure. Ras GTPase activity was measured in whole-lung homogenates, and in cytosolic and membrane subcellular fractions. Ras GTPase enzymatic activity was measured by ELISA. (**A**) In unfractionated whole-lung homogenate tissue, OVA-exposed mice have 2.61-fold greater total Ras GTPase activity compared with FA controls (**p = 0.0022 by *t test*). (**B**) FTI-277 treatment had no effect on Ras GTPase activity in either FA or OVA-exposed mice (p = NS by one-way ANOVA). The OVA groups have greater Ras activity than the FA control groups (2.28-fold difference in OVA plus PBS versus FA plus PBS, p = NS; and 2.92-fold difference in OVA plus FTI versus FA plus FTI *$p < 0.05$ by one-way ANOVA). (**C**) Comparing groups by subcellular fraction, Ras GTPase activity is higher in the cell membrane fractions as compared with cytosolic fractions for both the OVA and FA groups (OVA [cytosolic] versus OVA [membrane], p = NS; FA [cytosolic] versus FA [membrane], ***$p < 0.001$ by one-way ANOVA). In both the cytosolic and membrane fractions comparing OVA versus FA, Ras GTPase activity was significantly greater in the OVA groups (OVA [cytosolic] versus FA [cytosolic], *$p < 0.05$; OVA [membrane] versus FA [membrane], **$p < 0.01$ by one-way ANOVA). (**D**) In OVA-exposed mice, treatment with FTI-277 did not affect Ras enzyme activity in the membrane or cytosolic fractions for both groups (OVA plus PBS [cytosolic] versus OVA plus PBS [membrane], and OVA plus FTI [cytosolic] versus OVA plus FTI [membrane], p = NS for all comparisons by one-way ANOVA). Ras GTPase activity in the cytosolic fraction of the OVA plus PBS group was significantly higher than the FA plus PBS control (OVA plus PBS [cytosolic] versus FA plus PBS [cytosolic], *$p < 0.01$ by one-way ANOVA). The membrane fraction had a significantly greater Ras GTPase activity as compared with the cytosolic fraction in the FA plus PBS group (FA plus PBS [cytosolic] versus FA plus PBS [membrane], *$p < 0.05$ by one-way ANOVA), but this effect was only a trend in the FTI-277–treated FA mice (FA plus FTI [cytosolic] versus FA plus FTI [membrane], p = NS by one-way ANOVA). Ras GTPase activity units were natural logarithm transformed prior to analysis. The graph shows transformed data and therefore displays arbitrary units. (**E**) Ras GTPase activity demonstrated a positive linear correlation with BALF total inflammatory cell count (r^2 = 0.75, p = 0.0006, confidence interval [CI] 0.0239–0.0615) and with BALF absolute (abs.) eosinophil count (r^2 = 0.62, p = 0.0072, CI 0.0165–0.076). Total Ras activity of combined membrane and cytosolic fractions are plotted.

functioning of FTase and access to the FPP substrate to catalyze the Ras farnesylation reaction. We therefore hypothesized that inhibition of FTase with FTI-277 would disrupt Ras signaling and attenuate allergic airway inflammation in OVA-exposed mice. We measured the effect of FTI-277 on OVA-induced allergic inflammation by measuring BALF leukocyte counts and cytokine levels, goblet cell hyperplasia, and histopathologic peribronchiolar inflammation by semiquantitative scoring.

In our model of OVA-induced allergic inflammation, the eosinophil is the predominant leukocyte typically representing 70–80% of the BALF total leukocyte counts. In OVA-exposed mice, there was a trend of increased BALF total live cell count with FTI-277 treatment, but this did not achieve statistical significance (p = NS by one-way ANOVA) (Fig. 4A). Measured another way using BALF total inflammatory cells per 10 high-power fields, FTI-277 treatment of OVA-exposed mice increased inflammatory cell influx by 1.72-fold (*$p < 0.05$ by one-way ANOVA, Fig. 4A). Thus, contrary to our hypothesis, in OVA-exposed mice, treatment with FTI-277 caused a significant increase in total inflammatory cells present in BALF (Fig. 4A) with a 2.58-fold increase in eosinophil numbers as compared with the vehicle control group (*$p < 0.01$ by one-way ANOVA, Fig. 4B). However, treatment of OVA mice with FTI-277 did not significantly affect BALF macrophage, lymphocyte, or neutrophil cell counts as compared with OVA plus PBS controls (p = NS, data not shown).

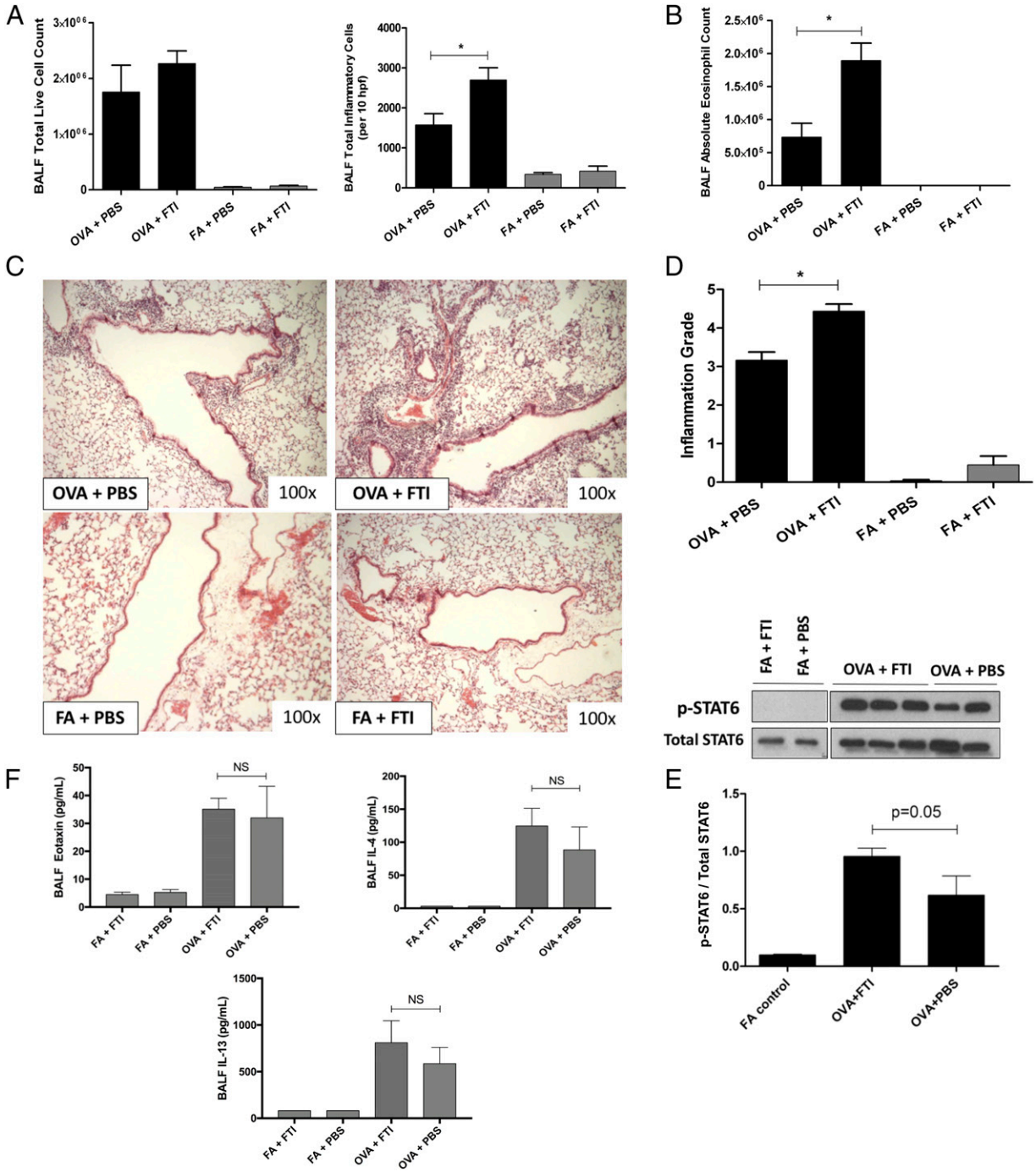

FIGURE 4. FTase inhibition with FTI-277 exacerbates allergic airway inflammation in a IL-4/IL-13/STAT6/eotaxin-independent manner. BALB/c mice were sensitized to OVA and then challenged with 1% OVA aerosol or FA six times over a 2 wk period. Mice were injected daily with FTI-277 (20 mg/kg per day, i.p.) before each OVA aerosol exposure. To assess for inflammation and drug effect, we quantified total and differential inflammatory cell counts and chemokines and cytokines in BALF, assessed histopathology and inflammation grade by H&E staining, and measured total and phosphorylated STAT6 in whole-lung homogenate by Western blot. (**A**) In OVA-exposed mice, treatment with FTI-277 did not significantly increase BALF total live cell count (p = NS by one-way ANOVA). However, measured as BALF total inflammatory cells per 10 high-power fields, FTI-277 treatment of OVA-exposed mice increased inflammatory cell influx by 1.72-fold ($*p < 0.05$ by one-way ANOVA). Treatment with FTI-277 had no detectible proinflammatory effects in any of the FA control groups. (**B**) Treatment with FTI-277 increased BALF absolute eosinophil count by 2.58-fold (OVA plus PBS versus OVA plus FTI, $*p < 0.01$ by one-way ANOVA). (**C**) H&E-stained lung sections indicate that treatment with FTI-277 augmented peribronchial and perivascular inflammation in the OVA-exposed mice. (**D**) Semiquantification of the H&E sections corresponded to a 1.40-fold increase in the inflammation grade ($*p < 0.001$ by one-way ANOVA). There were no statistically significant effects of FTI-277 on inflammation grade in the FA-exposed control groups. (**E**) In OVA-exposed mice, there was a significant increase in STAT6 phosphorylation as compared with FA controls. Treatment with FTI-277 further increased OVA-induced STAT6 phosphorylation by 1.55-fold, but this was not statistically significant (OVA plus PBS versus OVA plus FTI, $p = 0.05$ by one-way ANOVA). (**F**) Cytokines IL-4 and IL-13 induce phosphorylation of the transcription factor STAT6, which then activates the transcription of eotaxin. To assess this, we measured peptide levels of secreted IL-4, IL-13, and eotaxin in BALF. There were no statistically significant differences in BALF eotaxin levels (p = NS by one-way ANOVA) with FTI-277 treatment in either FA or OVA groups. The cytokine IL-4 was significantly induced in BALF upon OVA exposure (OVA plus FTI versus FA plus FTI, $p = 0.0371$ by one-way ANOVA), however, there were no statistically significant differences in BALF IL-4 levels with FTI-277 treatment in either FA or OVA groups (p = NS by one-way ANOVA). There were no statistically significant differences in BALF IL-13 levels with FTI-277 treatment in either FA or OVA groups (p = NS by one-way ANOVA).

The effect of FTI-277 treatment on BALF inflammatory cell numbers was supported by visual scoring of peribronchial and perivascular inflammation using H&E-stained histopathological lung sections. There was a marked increase in perivascular and peribronchiolar inflammatory cell infiltrate in OVA mice treated with FTI-277 compared with OVA-exposed mice treated with drug vehicle (Fig. 4C, 4D). No significant changes in inflammation were observed in the FA controls (Fig. 4C, 4D). The presence of significant eosinophilic infiltration with moderate, multifocal perivascular, and peribronchiolar to interstitial lymphoplasmacytic infiltration, few neutrophils, and limited alveolar histiocytosis was confirmed by an independent veterinary pathologist at University of California, Davis.

Given that our mouse model manifests a strong Th2 allergic response with high IL-13 production (6), we expected activation of STAT6 signaling in lung tissues. As predicted, mice exposed to OVA showed robust STAT6 phosphorylation relative to FA controls, which had no STAT6 phosphorylation (in homogenized whole-lung tissue) ($p < 0.05$ by one-way ANOVA, Fig. 4E). OVA mice treated with FTI-277 had a 1.55-fold increase in STAT6 phosphorylation as compared with OVA control; however, this did not reach statistical significance ($p = 0.05$ by one-way ANOVA, Fig. 4E). FA-exposed mice treated with FTI-277 or drug vehicle control showed no significant difference in STAT6 phosphorylation. To assess both the downstream chemokine targets of the STAT6 transcription factor and upstream STAT6-inducing cytokines, we measured eotaxin (downstream) and IL-4 and IL-13 (upstream) secreted peptide levels in the BALF. Surprisingly, BALF eotaxin levels were not significantly increased with FTI-277 treatment in the OVA groups (p = NS by one-way ANOVA, Fig. 4F). Similarly, BALF IL-13 and IL-4 levels were not significantly increased with FTI-277 treatment in the OVA groups (p = NS by one-way ANOVA, Fig. 4F). These results suggest that the increase in eosinophilic inflammation observed with FTI-277 treatment in the OVA group may occur by a IL-4/IL-13/STAT6/eotaxin–independent mechanism.

BALF cytokine levels

We measured a total of 32 cytokines in BALF supernatant using a multiplex assay. Treatment with FTI-277 did not have a statistically significant effect on the levels of the following BALF cytokines and chemokines: IL-5, IL-10, IL-1α, IL-1β, IL-2, IP-10, IL-12, MCP-1, IL-9, VEGF, KC, G-CSF, LIX, MIP-1α, MIP-1β, MIG, LIF, M-CSF, RANTES, IL-17, IL-3, IL-7, IL-12, IL-15, GM-CSF, IFN-γ (data not shown). There were no significant differences in any of the cytokines analyzed between FTI-277–treated and vehicle-treated mice in the FA groups. However, in OVA exposed mice, treatment with FTI-277 reduced IL-6 concentration by 67.4% (*p = 0.0258), MIP-2 by 46.3% (*p = 0.0356), and TNF-α by 49.6% (*p = 0.05), all analyzed by one-way ANOVA (Fig. 5). These three cytokine and chemokine data appear to contradict the other measurements of inflammation showing greater allergic inflammation with FTI-277 treatment.

Goblet cell hyperplasia

Airway epithelial remodeling, which includes goblet cell metaplasia and hyperplasia, is a cardinal feature of allergic asthma in both animal models and human disease. We hypothesized that treatment with FTI-277 would reduce positive PAS staining of goblet cells in mice exposed to OVA. Using a semiquantitative scoring method, we observed that FTI-277 increased goblet cell metaplasia and hyperplasia in the OVA group (p = 0.025, by t test; Fig. 6A, 6B). FA mice showed no significant change with FTI-277 or vehicle treatment (Fig. 6B).

Lung physiology

In an MCh dose–response aerosol challenge, OVA-exposed mice typically manifest heightened baseline Rrs, decreased baseline Cdyn, and increased AHR, as indicated by increased airway resistance at any given dose of MCh relative to their respective FA controls. We hypothesized that treatment with FTI-277 would attenuate OVA-induced airway hyperresponsiveness and improve dynamic lung compliance.

Contrary to our hypothesis, treatment with FTI-277 in the OVA group caused a statistically significant increase in Rrs and AHR at all three MCh doses (Fig. 7A) and a statistically significant decrease in Cdyn, but only at the highest MCh dose of 2 mg/ml, relative to their respective control group OVA plus PBS (Fig. 7B). There were no statistically significant changes due to FTI-277 treatment in the FA groups. There was no evidence of significant interaction between the treatment group and the MCh challenge dose for either Cdyn or Rrs analyses (p = NS by two-way ANOVA).

Alveolar-capillary membrane barrier integrity

Because of both the unexpected proinflammatory effects of FTI-277 and the simultaneous yet paradoxical decrease in BALF cytokines (IL-6, MIP-2, TNF-α), we assessed whether this drug had any significant and direct pulmonary toxic effects independent of inflammation. We measured albumin levels in BALF supernatant as

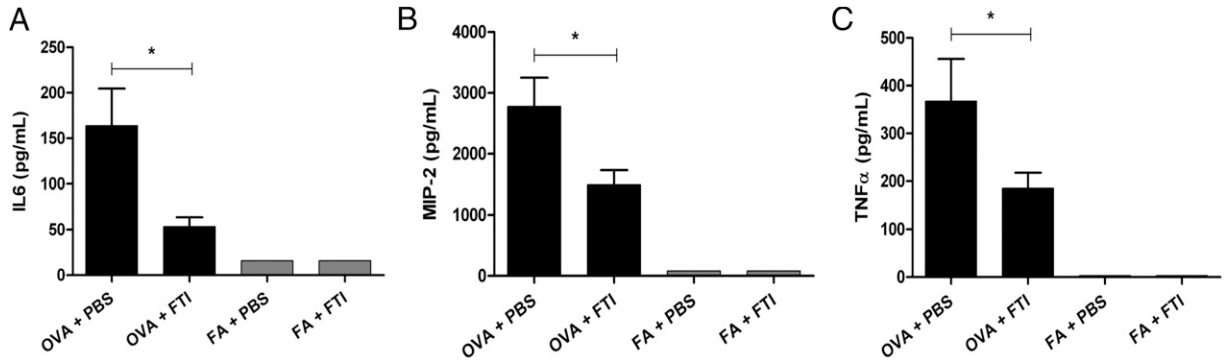

FIGURE 5. Effect of FTI-277 on select BALF cytokine levels. BALB/c mice were sensitized to OVA and then challenged with 1% OVA aerosol or FA six times over a 2 wk period. Mice were injected daily with FTI-277 (20 mg/kg per day, i.p.) before each OVA aerosol exposure. BALF supernatant was collected for multiplex analysis for select cytokines and chemokines. Treatment with FTI-277 reduced cytokine levels of IL-6, MIP-2, and TNF-α (see the *Results* for the rest of the cytokine and chemokine measures, which did not reach significance). In the OVA group, treatment with FTI-277 reduced cytokine concentrations in BALF by the following amounts: (**A**) IL-6 by 67.4% (*p = 0.0258), (**B**) MIP-2 by 46.3% (*p = 0.0356), and (**C**) TNF-α by 49.6% (*p = 0.05), all analyzed by one-way ANOVA. There were no significant changes in the FA control groups.

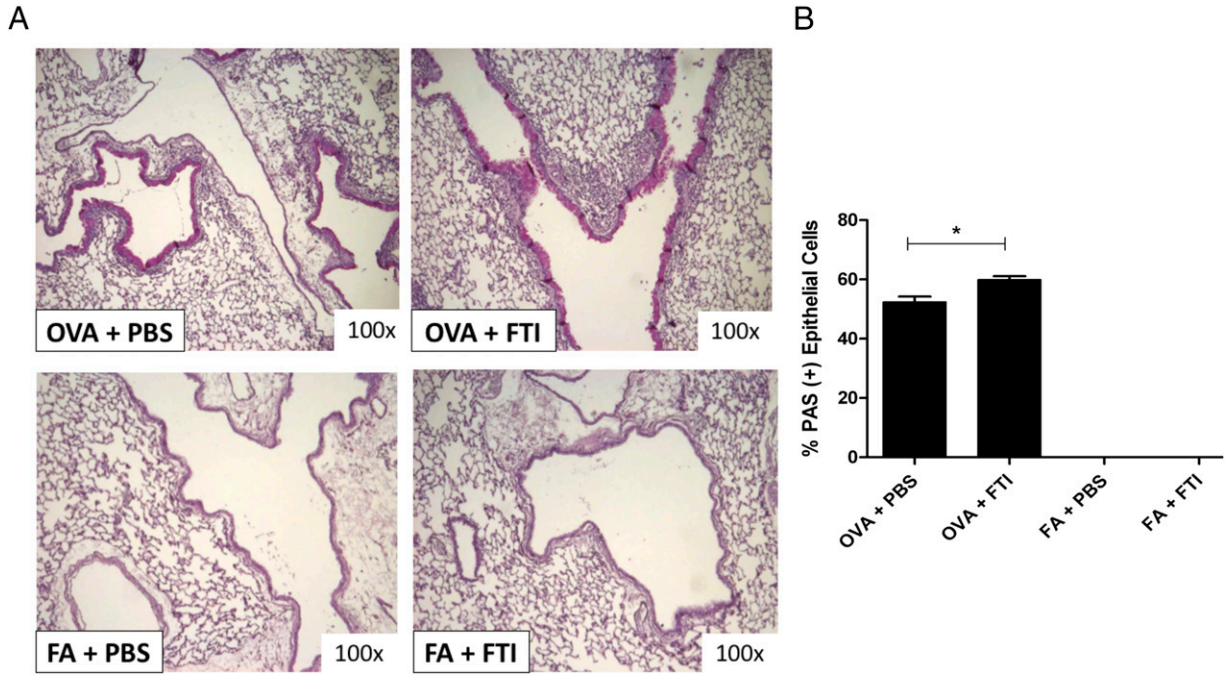

FIGURE 6. FTase inhibition with FTI-277 increases airway goblet cell hyperplasia. BALB/c mice were sensitized to OVA and then challenged with 1% OVA aerosol or FA six times over a 2 wk period. Mice were injected daily with FTI-277 (20 mg/kg per day, i.p.) before each OVA aerosol exposure. PAS staining of lung sections was used to assess the degree of goblet cell metaplasia and hyperplasia as a measure of airway epithelial remodeling and mucus production. (**A**) PAS staining of lung sections showed that treatment with FTI-277 further increases OVA-induced goblet cell metaplasia and hyperplasia in the airway epithelium. (**B**) Percentage of PAS positive airway epithelial cells increased by 1.14-fold (*p = 0.025 by t test) with FTI-277 treatment as compared with OVA plus PBS controls. There were virtually no goblet cells present in the conducting airways of mice exposed to FA in both the PBS and FTI-277-treated groups.

an indicator of alveolar-capillary membrane (ACM) barrier integrity because the loss of endothelial-alveolar barrier integrity would allow albumin to pass into the airspace, becoming detectible in lavage fluid.

Exposure to OVA greatly increased BALF albumin concentration relative to FA groups, indicating a loss of ACM barrier integrity during allergic inflammation alone (Fig. 8A, 8C). There was a statistically significant positive linear correlation between BALF albumin concentration and BALF total cell counts (Fig. 8B), but treatment with FTI-277 did not significantly increase albumin levels between untreated controls and drug-treated mice for both OVA and FA groups (Fig. 8C). This indicates that treatment with FTI-277 did not directly cause any significant injury to the ACM. Treatment with FTI-277, therefore, did not contribute to leukocyte leakage into the airspace or to inflammation by direct cytotoxic mechanisms.

Drug tolerability

Treatment with FTI-277 did not hinder normal weight gain in mice in either the OVA- or FA-exposed groups. Average weights (± SEM) were

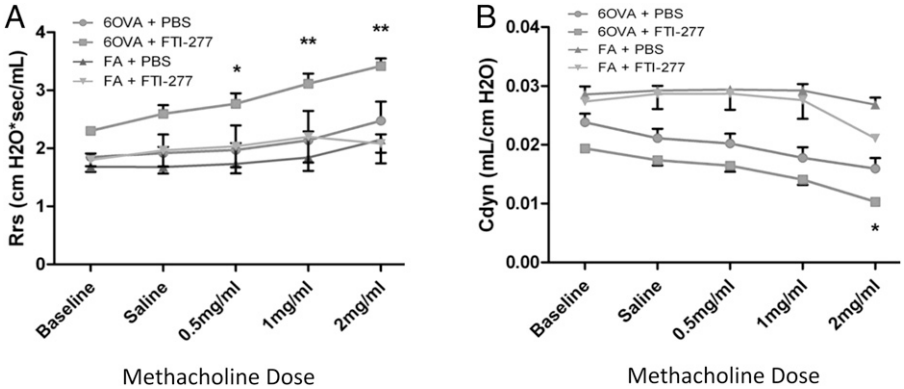

FIGURE 7. FTase inhibition with FTI-277 exacerbates AHR and decreases lung compliance. BALB/c mice were sensitized to OVA and then challenged with 1% OVA aerosol or FA six times over a 2 wk period. Mice were injected daily with FTI-277 (20 mg/kg per day, i.p.) before each OVA aerosol exposure. Before and after increasing doses of MCh, lung physiology was measured in all treatment groups to assess the effects of FTI-277 treatment on respiratory function. (**A**) There were no significant baseline differences in Rrs between OVA plus PBS versus OVA plus FTI (p = NS by two-way ANOVA). Treatment with FTI-277 increased Rrs and AHR at all three doses of MCh (*$p < 0.05$ for OVA plus PBS versus OVA plus FTI; **$p < 0.01$ for OVA plus PBS versus OVA plus FTI). The greatest difference in Rrs was seen between OVA plus PBS versus OVA plus FTI at the highest dose of MCh (2 mg/ml). There were no statistically significant differences in Rrs in FA controls ± FTI-277 treatment (FA plus PBS versus FA plus FTI; p = NS). (**B**) There were no baseline differences in Cdyn between OVA plus PBS versus OVA plus FTI (p = NS by two-way ANOVA). Treatment with FTI-277 decreases Cdyn (*$p < 0.05$ for OVA plus PBS versus OVA plus FTI) at the highest dose of MCh (2 mg/ml). There were no statistically significant differences in Cdyn in FA controls ± FTI treatment (FA plus PBS versus FA plus FTI; p = NS). All analyses were done by two-way ANOVA with posttest corrections.

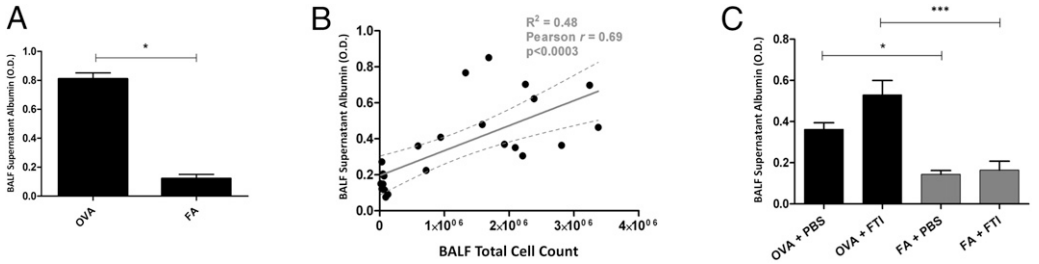

FIGURE 8. The effects of FTI-277 treatment on ACM barrier integrity. BALB/c mice were sensitized to OVA and then challenged with 1% OVA aerosol or FA six times over a 2 wk period. Mice were injected daily with FTI-277 (20 mg/kg per day, i.p.) before each OVA aerosol exposure. We measured BALF albumin concentration as an indicator of ACM barrier health in our model and to assess for endothelial or epithelial toxicity due to FTI-277. Data are represented as OD at a wavelength of 450 nm. (**A**) Sensitization followed by exposure to nebulized OVA alone induces vascular leak of albumin into the alveolar compartment, indicating relative ACM barrier injury. Albumin increased by 6.7-fold in OVA-exposed mice as compared with FA-exposed mice ($*p = 0.0055$ by t test). (**B**) BALF supernatant albumin levels positively correlate with BALF total cell count ($p < 0.0003$, $r^2 = 0.48$, Pearson $r = 0.69$, 95% confidence interval of 7.3×10^{-8} to 2.04×10^{-7}). (**C**) Treatment with FTI-277 does not result in a statistically significant change in BALF albumin levels in both the OVA and FA groups (OVA plus PBS versus OVA plus FTI, and FA plus PBS versus FA plus FTI; p = NS by one-way ANOVA for both comparisons). Similar to (A), the OVA groups had significantly higher levels of BALF albumin independent of FTI treatment (OVA plus PBS versus FA plus PBS; $*p < 0.05$ by one-way ANOVA; OVA plus FTI versus FA plus FTI; $***p < 0.001$ by one-way ANOVA). These data indicate that FTI-277 treatment alone did not independently compromise ACM barrier integrity.

as follows: OVA plus PBS = 28.4 ± 0.25, OVA plus FTI = 28.2 ± 0.06, FA plus PBS = 28.0 ± 0.23, FA plus FTI = 28.2 ± 0.23 (p = NS by one-way and two-way ANOVA). Of note, weight alone as a single indicator of systemic toxicity is not a detailed enough measure to completely rule out subtle organ damage or other toxic drug effects, but weight gain is generally considered a reliable measure of good health and drug tolerability in experimental mice (39).

Ras farnesylation in HBE1 cells

To further investigate the effects of FTI-277 in a single-cell type without the more complex in vivo situation, we used the HBE1 cell line. We selected human bronchial epithelial cells given their central role in the pathogenesis of human asthma (40–42), and our established IL-13 in vitro model of mucosal Th2 inflammation (11, 43). We first confirmed that, at pharmacologically relevant doses, FTI-277 inhibits FTase by measuring Ras translocation between cell plasma membrane and cytosol in ultra-centrifuged subcellular fractions.

Based on the knowledge that farnesylation is necessary for Ras GTPase membrane anchoring, we treated HBE1 cells with FTI-277 (10 or 20 μM for 30 min) or drug vehicle and determined the proportion of subcellular membrane versus cytosolic Ras (Fig. 9). Total Ras represents the sum of the membrane and cytosolic fractions, previously determined in separate exploratory experiments to be equivalent to the direct measurement of total Ras by Western blot of unfractionated total cell homogenates. Without FTI-277 treatment, Ras is predominantly present in the cell membrane (Fig. 9A). Treatment with FTI-277 changed the ratio of membrane to cytosolic Ras in a dose-dependent manner, showing

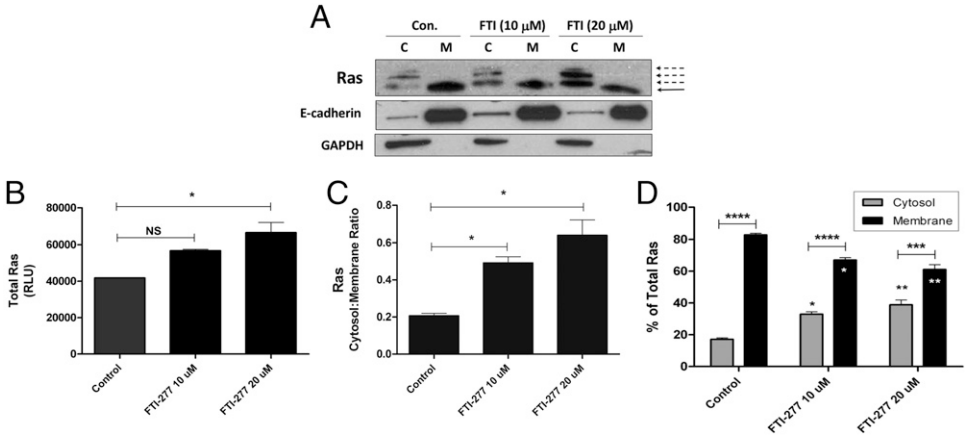

FIGURE 9. Subcellular localization of Ras in HBE1 cells and the effects of FTI-277 treatment. HBE1 human bronchial epithelial cells were treated with FTI-277 (10 and 20 μM) or control drug vehicle for 30 min. Cell homogenates underwent high speed ultracentrifugation to separate them into cytosolic and membrane subcellular fractions. Ras protein for each treatment group was assessed by Western blot. Ras semiquantitative values were normalized using E-cadherin and GAPDH for membrane and cytosolic fractions, respectively. A total of $n = 3$ independent experiments were conducted of which a representative gel is shown. FTI = FTI-277. (**A**) In the untreated control, Ras protein is highly expressed and is localized predominantly in the cell membrane fraction (solid black arrow). Treatment with FTI-277 increases Ras protein in the cytosolic fraction while decreasing Ras in the membrane fraction in a dose-dependent manner. The additional bands seen in the cytosolic fractions represent increasing proportions of unfarnesylated Ras protein with increasing FTI-277 dose (dashed black arrows). (**B**) Treatment with FTI-277 caused a dose-dependent increase in total Ras protein expression (Control versus FTI 10 μM [p = NS]; Control versus FTI 20 μM [$*p < 0.05$ by one-way ANOVA]). (**C**) Plotted as cytosol/membrane ratio, the cytosolic fraction of Ras increased relative to the membrane fraction with increasing doses of FTI-277 (control versus FTI 10 μM, $*p = 0.02$; control versus FTI 20 μM, $*p = 0.02$ by one-way ANOVA). (**D**) Plotted as percentage of total Ras, treatment with FTI-277 resulted in a statistically significant increase in cytosolic Ras corresponding with a decrease in membrane-associated Ras. Cytosol versus membrane comparisons within each treatment group showed the following: control ($****p < 0.0001$ by two-way ANOVA), FTI 10 μM ($****p < 0.0001$), and FTI 20 μM ($***p < 0.001$). For cytosolic and membrane comparisons across each treatment group, respectively: control versus FTI 10 μM ($*p < 0.05$ by one-way ANOVA), control versus FTI 20 μM ($**p = 0.0098$), and FTI 10 μM versus FTI 20 μM (p = NS).

greater cytosolic and lower membrane Ras, as expected (Fig. 9A, 9C, 9D). Treatment with FTI-277 also increased the expression of total Ras (Fig. 9B). The additional two bands seen above the lowest band in the Ras cytosolic fractions (Fig. 9A, dashed black arrows) represent other unfarnesylated Ras proteins and isoforms (44), which also increase in a dose-dependent manner with FTI-277 treatment. By contrast, farnesylated Ras protein is membrane bound (Fig. 9A, solid black arrow). These data confirm the drug's known mechanism of action in the FTI-277 doses used in our in vitro experiments (i.e., the inhibition of Ras farnesylation).

Effects of FPP and FTI-277 on Eotaxin-3 secretion in HBE1 epithelial cells

IL-13 is a major cytokine important in human asthma in which IL-13 antagonists are currently being studied as potential treatment for asthma (45). IL-13 induces eotaxin gene expression in endothelial and epithelial cells via the transcription factor STAT6 (15, 46–51). The three human eotaxins (eotaxin-1 [CCL11], eotaxin-2 [CCL24], eotaxin-3 [CCL26]) are potent chemokines for the recruitment of eosinophils into the lung and airway tissues (50–55). Of these three eotaxins, eotaxin-2 and eotaxin-3 are most relevant to human severe asthma; both are known to persist despite treatment with corticosteroids (27, 55). Eotaxin-3 in particular has the best correlation with other biomarkers of Th2 high inflammation in human asthma (26, 56, 57). We therefore chose to study the IL-13/STAT6/eotaxin-3 signaling axis in our HBE1 cell experiments, given its clinical relevance.

We previously observed a decrease in eotaxin-3 secretion from HBE1 cells treated with the HMGCR inhibitor, simvastatin (11), and this statin inhibition occurred by an MA-dependent mechanism, implicating FPP, GGPP, and/or cholesterol pathways (Fig. 1). Given the potential role of FPP (58) and Ras in allergic asthma and the results from our mouse experiments, we wanted to determine if FTI-dependent inhibition had a similar effect on IL-13–induced eotaxin-3 secretion. To this end, HBE1 cells were pretreated with FTI-277 or FPP for 60 h followed by stimulation with IL-13 (+FTI-277 or +FPP) for the last 12 h to induce eotaxin-3 production and extracellular peptide secretion (total of 72 h exposure to FTI-277 [5, 10, and 20 μM] and/or FPP [10 μM]). Given the known IC_{50} of 50 nM, we expected that with the micromolar doses of FTI-277 used (and 72 h treatment duration), all Ras GTPases would be fully inhibited. All IL-13/STAT6/eotaxin-3 experiments were done at a FTI-277 treatment duration of 72 h (Fig. 10). Effects of FPP and FTI-277 on eotaxin-3, STAT6, and Ras subcellular localization were confirmed in multiple experiments. Measurements were made on the same cell samples for Ras and STAT6 and their respective cell-free media for eotaxin-3 ELISA.

Unlike Fig. 9A, in which the unfarnesylated Ras proteins were visualized as multiple bands in the cytosolic fraction (dashed black arrows), in Fig. 10D and 10E, only one band is seen in the cytosolic fraction, which represents unfarnesylated Ras. The key difference between the experiments represented by Figs. 9 and 10 is the time point of 30 min versus 72 h, respectively.

In unstimulated and control HBE1 cells, treatment with FTI-277 or FPP had no effect on basal secretion of eotaxin-3 (Fig. 10A). As expected, IL-13 stimulation of HBE1 cells increased eotaxin-3 secretion by 11.3-fold compared with unstimulated control cells. In contrast to the effects of simvastatin (6, 11), treatment of HBE1 cells with FTI-277 had no significant effect on IL-13–induced eotaxin-3 peptide secretion (Fig. 10A) or STAT6 phosphorylation (Fig. 10B). This is consistent with the lack of inhibition of eotaxin-3 secretion because STAT6 controls eotaxin-3 gene expression. However, exogenous treatment of IL-13–stimulated cells with the MA metabolite FPP unexpectedly and significantly increased STAT6 phosphorylation by 1.53-fold ($*p < 0.05$ by one-way ANOVA, Fig. 10C) and augmented eotaxin-3 secretion by 3.2-fold compared with IL-13 alone ($**p < 0.001$ by one-way ANOVA, Fig. 10A). As the graph shows, this is consistent with a synergistic effect of combined IL-13 plus FPP on eotaxin-3 secretion, as compared with IL-13 and FPP separately.

Given the effects of FPP on IL-13–induced eotaxin-3 secretion and lack of eotaxin-3 inhibition by FTI-277, we evaluated the role of Ras subcellular localization (i.e., farnesylation) at this 72 h time point. For control groups, the majority of Ras was located in the cytosolic fraction (Fig. 10D, 10E, $*p < 0.05$ by two-way ANOVA), unlike at the 30 min time point at which the majority of Ras was in the membrane (Fig. 9A). Treatment with FPP, IL-13, or IL-13 plus FPP was associated with translocation of Ras from the cytosol to the membrane as compared with the control group (Fig. 10D, $^{f,\Phi}p = 0.0043$ by one-way ANOVA comparing cytosolic or membrane fractions across treatment groups; $**p < 0.0001$ by two-way ANOVA comparing cytosolic versus membrane fractions within each treatment group). However, there were no significant differences between the IL-13 and IL-13 plus FPP groups with respect to the subcellular localization of Ras. This suggests that the FPP-augmented IL-13–induced STAT6 phosphorylation (Fig. 10C) and eotaxin-3 secretion (Fig. 10A) occurs by a mechanism independent of changes in Ras farnesylation (Fig. 11).

With respect to treatment with FTI-277, this caused an unexpected and paradoxical increase in the membrane fraction as compared with cytosol at this 72 h time point (Fig. 10E, $**p < 0.01$ by two-way ANOVA). Based on the known mechanism of action of FTI-277 (Fig. 1), we had expected an increase in the cytosolic fraction and a decrease in the membrane fraction of Ras, as we saw in Fig. 9. Treatment with IL-13 induced translocation of Ras from the cytosol to the membrane as compared with the control group (Fig. 10E, $^{f,\Phi}p = 0.0385$ by one-way ANOVA comparing cytosolic or membrane fractions between treatment groups for IL-13 only; $**p < 0.01$ by two-way ANOVA comparing cytosolic versus membrane fractions for the IL-13 and FTI treatment groups). Like the FPP experiment above, there were no statistically significant differences between the IL-13 and IL-13 plus FTI groups with respect to the cellular localization of Ras. This confirms that at the 72 h time point, treatment with FTI-277 failed to significantly affect the subcellular location of Ras in the expected manner (i.e., increase cytosolic Ras and decrease membrane Ras), unlike at the 30 min time point at which it did inhibit Ras farnesylation and thereby depleted Ras from cell membranes while enriching cytosolic Ras (Fig. 9).

These are key findings because pharmacologic inhibition of FTase does the following: 1) blocks Ras farnesylation and therefore inhibits Ras membrane enrichment (Fig. 1) and subsequent kinase-mediated signal transduction and 2) blocks the use of FPP thereby increasing local intracellular FPP concentrations. There are several important implications of these two effects, which we address in the *Discussion*, where we also explore potential alternative interpretations of these data (Fig. 11).

Discussion

We sought to determine whether pharmacological inhibition of FTase with FTI-277, a potent Ras CaaX domain peptidomimetic, attenuates OVA-induced allergic inflammation, epithelial remodeling, and AHR, as well as reduces Ras GTPase activity. This is the only study we are aware of that systematically assesses the therapeutic potential of FTase inhibition in a murine model of asthma and in an in vitro model of epithelial type 2 immune activation using human bronchial epithelial cells.

Our hypothesis derives from our understanding of the biochemistry of the MA pathway and its two basic arms, the nonsterol (i.e., isoprenoid) and sterol (i.e., squalene and cholesterol) arms

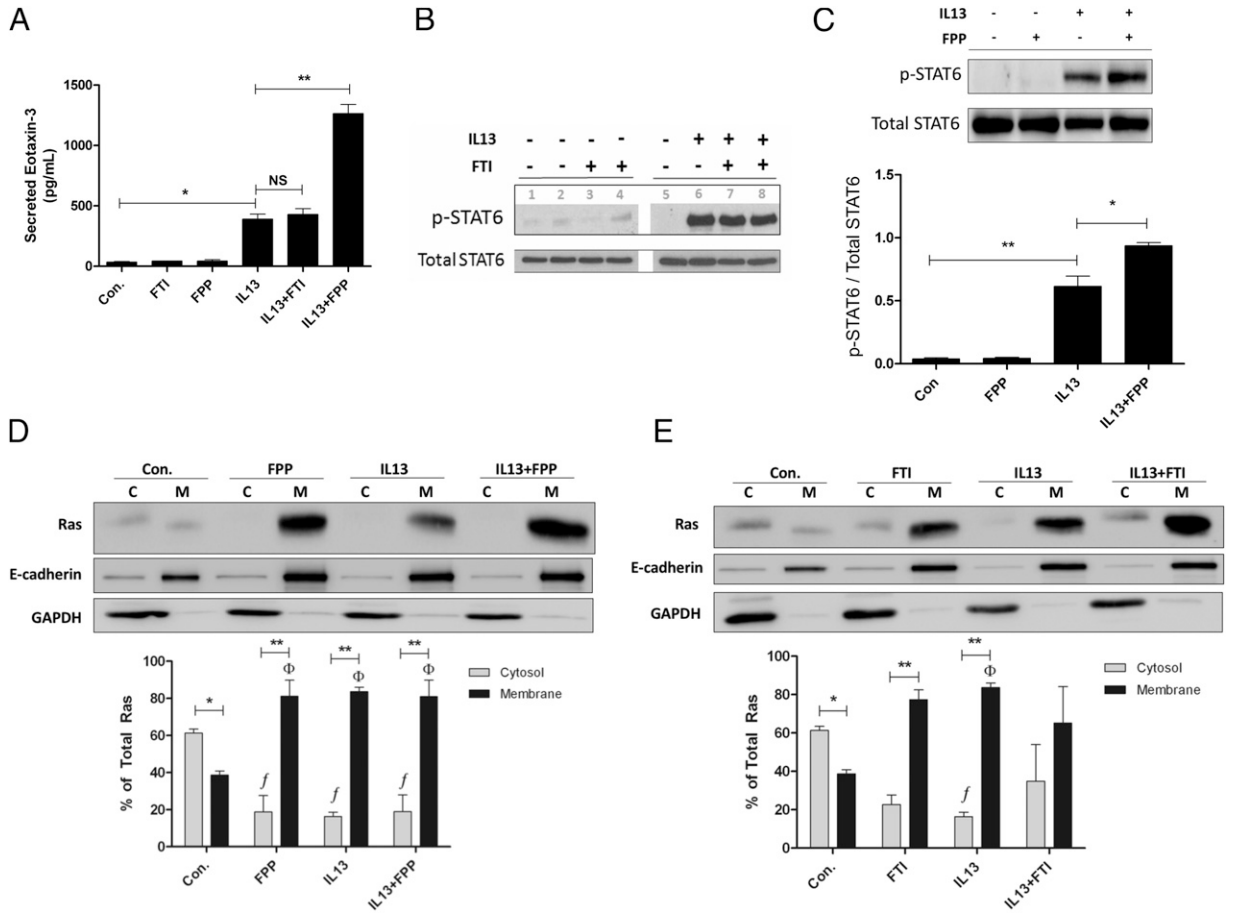

FIGURE 10. Effects of FTI-277 and FPP on IL-13–induced Eotaxin-3 secretion and STAT6 phosphorylation in HBE1 cells. HBE1 human bronchial epithelial cells were pretreated with FTI-277 (5, 10, or 20 μM) or FPP (10 μM) for 60 h, then stimulated with IL-13 for another 12 h (72 h total). Cell-free media were then collected to measure secreted eotaxin-3 peptide by ELISA. Total cell homogenates were collected for total- and *p*-STAT6, and cell membrane and cytosolic subcellular fractions for Ras expression by Western blot. Ras semiquantitative values were normalized using E-cadherin and GAPDH for membrane and cytosolic fractions, respectively. A total of $n = 3$ independent experiments were conducted of which representative gels are shown. FTI = FTI-277. (**A**) Stimulation of HBE1 cells with IL-13 resulted in an 11.3-fold increase in eotaxin-3 secretion (control versus IL-13, $*p < 0.001$ by one-way ANOVA). Pretreatment of HBE1 cells with FTI-277 (20 μM) did not affect IL-13–induced eotaxin-3 secretion (p = NS). Although exposure to FPP (10 μM) by itself had no effect on basal eotaxin-3 production, FPP augmented IL-13–induced eotaxin-3 secretion by 3.2-fold (IL-13 versus IL-13 plus FPP, $**p < 0.001$ by one-way ANOVA). (**B**) Stimulation of HBE1 cells with IL-13 induced STAT6 phosphorylation (p-STAT6). Pretreatment with FTI-277 (5 and 10 μM) did not affect STAT6 phosphorylation. Gel lanes 3 and 7 were treated with 5 μM of FTI-277. Gel lanes 4 and 8 were treated with 10 μM of FTI-277. (**C**) Stimulation of HBE1 cells with IL-13 caused a 16.3-fold increase in p-STAT6 relative to total STAT6 ($**p < 0.01$ by one-way ANOVA). Although FPP (10 μM) had no effect on basal STAT6 phosphorylation, FPP augmented IL-13–induced p-STAT6 by 1.53-fold (IL-13 versus IL-13 plus FPP, $*p < 0.05$ by one-way ANOVA). (**D**) In untreated control cells, Ras was predominantly in the cytosol ($*p < 0.05$ by two-way ANOVA), whereas treatment with FPP (10 μM), IL-13, or IL-13 plus FPP caused a relative increase in membrane Ras with a complementary decrease in cytosolic Ras ($**p < 0.0001$ by two-way ANOVA) as compared with the control group ($^{f,\Phi}p = 0.0043$ by one-way ANOVA). There was no significant difference in Ras localization between IL-13 and IL-13 plus FPP. Membrane (E-cadherin) and cytocolic (GAPDH) loading controls indicate appropriate separations for cytosolic and membrane subcellular fractions for Ras protein comparisons. (**E**) In untreated control cells, Ras was predominantly in the cytosol ($*p < 0.05$ by two-way ANOVA), whereas treatment with FTI (20 μM) and IL-13 independently caused a relative increase in membrane Ras and decrease in cytosolic Ras ($**p < 0.01$ by two-way ANOVA) as compared with the control group ($^{f,\Phi}p = 0.0385$ by one-way ANOVA for IL-13 only, p = NS for FTI). There was no statistically significant difference between IL-13 and IL-13 plus FTI. Membrane (E-cadherin) and cytosolic (GAPDH) loading controls indicate appropriate separations for cytosolic and membrane subcellular fractions for Ras protein comparisons.

(Fig. 1). Increasingly, there is greater appreciation that the MA pathway plays a critical role in adaptive immune responses, T cell polarity and proliferation, and Th2-mediated allergic inflammation (6, 59, 60).

Given that HMGCR inhibitors (e.g., statins) and GGTase inhibitors have been previously shown to mitigate allergen-induced airway inflammation in animal models (6, 16, 18, 24, 25, 61) and given the Th2 proinflammatory role of Ras in eosinophil biology and allergic inflammation (19, 21, 23), we reasoned that inhibiting FTase activity would indirectly inhibit Ras GTPase signaling by blocking Ras farnesylation (Fig. 1). Without this farnesyl tail, Ras cannot anchor in cell membranes, rendering it functionally inactive, thus, inhibiting Ras-mediated downstream signal transduction (62–64). Therefore, our hypothesis predicted that FTase inhibition would inhibit Ras-mediated allergic eosinophilic inflammation and the development of experimental asthma.

Our main findings can be summarized as follows: in naive noninflamed mouse lungs, Ras protein is located predominantly in cell membranes (Fig. 2), where it is enzymatically active (Fig. 3). This indicates that Ras is constitutively active in vivo and participates in normal homeostatic respiratory cellular physiology. Contrary to our hypothesis, inhibition of Ras farnesylation via pharmacologic antagonism of FTase using FTI-277 further exacerbates allergic airway inflammation (Fig. 4) and goblet cell

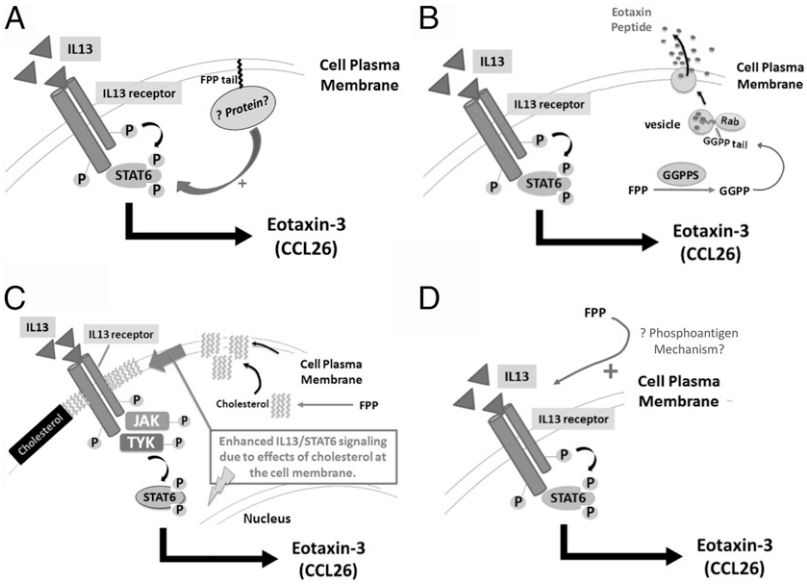

FIGURE 11. Hypothetical mechanisms of how FPP could augment IL-13–mediated signaling in human airway epithelial cells. Adding FPP exogenously to HBE1 cells caused a marked and unexpected increase in IL-13–mediated STAT6 activation, resulting in greater eotaxin-3 extracellular peptide secretion. The mechanism underlying this dramatic effect of FPP is not known. We propose four potential mechanisms that can be explored in forthcoming experiments to elucidate this important observation. (**A**) Increased farnesylation of a protein with the CaaX motif by FTase, which then enhances IL-13–mediated STAT6 phosphorylation and subsequent eotaxin-3 production. (**B**) FPP is converted to GGPP by GGPP synthase, which then geranylgeranylates Rab GTPases to promote vesicular secretion (or exocytosis) of eotaxin-3 peptide. (**C**) FPP is metabolized to squalene then to cholesterol, which enhances cell plasma membrane rigidity via increased lipid microdomains and rafts, and subsequent enhanced IL-13R/IL-13 ligand stability, leading to augmented IL-13 signaling and greater eotaxin-3 production. (**D**) FPP acts like a phosphoantigen via the butyrophilin receptor family to augment IL-13–mediated STAT6 phosphorylation and eotaxin-3 production in bronchial epithelial cells.

hyperplasia (Fig. 6) and worsens AHR (Fig. 7). Therefore, pharmacologic disruption of FTase activity and Ras farnesylation may be harmful as a therapeutic strategy in asthma. Our results may contradict previous work by other investigators who showed that Ras is a critical player in establishing the Th2 response in asthma (19, 21). In IL-13–stimulated HBE1 cells, FTase inhibition with FTI-277 did not affect Ras membrane and cytosol levels, IL-13/STAT6 signaling, or eotaxin-3 peptide secretion. However, the addition of exogenous FPP to these cells synergistically increased IL-13–induced STAT6 phosphorylation and eotaxin-3 peptide secretion (Fig. 10A–C), and this FPP effect occurs independent of Ras farnesylation (Fig. 10D). In summary, these data indicate that lung Ras GTPase is important in normal physiological function, inhibition of Ras farnesylation in vivo promotes Th2 inflammation and asthma pathogenesis, and excess FPP augments the proinflammatory effects of IL-13 on eotaxin-3 peptide secretion from airway epithelial cells. Our results highlight the complex role of the MA cascade in allergic inflammation relevant to human asthma and further suggest that rather than antagonizing FTase, depletion of FFP in the airways might confer therapeutic benefits in asthma (Fig. 11).

In support of this idea, inhibition of the enzyme FPP (or diphosphate) synthase (FPPS) by the bisphosphonate (BP) drug alendronate attenuates eosinophilic airway inflammation and suppresses eotaxin-2 production in lung macrophages (65). Being a key enzyme in the MA pathway, FPPS synthesizes FPP (Fig. 1), and therefore, alendronate acts similarly to statins in that both drugs reduce the pool of available FPP inside cells. Conversely, treatment with FTI-277 may increase the pool of available FPP (66), which can then be shunted to GGPP (Figs. 1, 11B). This in turn can increase geranylgeranylation of Rho, Ras, and/or Rab GTPases and can lead to increased cell signaling, proliferation, migration, vesicle trafficking and release, and inflammation (67–71). Thus, we speculate that diversion of FPP to other metabolites in the MA cascade is possible (Fig. 11B, 11C) among other potential mechanisms. Thus, FPP-enhanced IL-13/STAT6 signaling in airway epithelial cells may be a novel therapeutic target independent of Ras, worthy of further study.

MA- and FTase-dependent immune modulation

The MA pathway contributes to and regulates T cell–mediated immune responses, in particular APCs, dendritic cells, T cell activation (72, 73), and Th1/Th2 polarity (13, 59, 60). We previously showed that MA mediates Th2 allergic inflammation and lung eosinophilia in our mouse model (6). Simvastatin also inhibits T cell activation by impairing the function of Ras superfamily small GTPases, such as Ras, Rac, and Rab GTPase, key proteins activated by the isoprenoids FPP and GGPP (74) in the MA pathway (Fig. 1). Statins also negate Th2 allergic responses by reducing T cell activity and proliferation and IL-4/IL-13 cytokine production (4, 6, 75).

In our current study, however, although FTI-277 treatment did not significantly affect mouse BALF IL-4, IL-13, IL-5, or eotaxin levels, we did see significant amplification of eosinophilic inflammatory cell recruitment to the lung and increased airway remodeling as defined by goblet cell metaplasia and hyperplasia. Conversely, treatment with the FTI-277 reduced BALF levels of IL-6, MIP-2, and TNF-α (Fig. 5) despite the simultaneous increase in eosinophilic inflammation. Similarly, Xue et al. (76) noted a significant downregulation of Th1 cytokine secretion with the FTI, tipifarnib, including reductions in IL-6, IL-1β, and TNF-α, like we observed in our experiments. We speculate that by inhibiting Th1 polarity, FTI-277 indirectly enhanced Th2 responses, resulting in worsening eosinophilic inflammation. Another possible explanation is the temporal relationship between cytokines and infiltrating inflammatory cells, which may not be synchronized when we observe a single time point. Also, the proinflammatory effects of FTI-277 may not be occurring primarily via enhanced cytokine induction.

In our in vitro epithelial cell model, we chose to study IL-13–induced eotaxin-3 production as an indicator of type 2 inflammatory mucosal immune responses relevant to human asthma. The eotaxins (eotaxin-1 [CCL11], eotaxin-2 [CCL24], and eotaxin-3 [CCL26]) are well-characterized potent chemoattractants for systemic and tissue eosinophilia. Although FTI-277 treatment led to no significant changes in IL-13–induced STAT6 phosphorylation or eotaxin-3 secretion in HBE1 cells, the addition of exogenous FPP to HBE1 cells caused a significant increase in IL-13–induced STAT6 phosphorylation and eotaxin-3 secretion, and this occurred independent of Ras farnesylation (Fig. 10D). If farnesylation is playing an important role in this mechanism, then this suggests that farnesylation of a protein (or proteins) other than Ras (Fig. 11A) may be involved. Thus, Ras-independent protein farnesylation versus other direct FPP effects might be a novel mechanism and undiscovered part of the IL-13/STAT6/eotaxin signaling axis in airway epithelial cells (Fig. 11B, 11D).

Ras, FTase, and the role of FTI-277 treatment in allergic asthma

The Ras subfamily is a major intracellular signaling hub and functions to regulate many basic cellular processes. This includes signal transduction pathways involved in cellular proliferation, differentiation, polarization, cell growth, and cell motility important in cell biology, health, and disease (2, 12, 13, 36, 66, 77–82) in addition to the fundamental role that Ras plays in many cancers (2, 83–88). The FTase enzyme recognizes the CaaX box motif on the C terminus of Ras, covalently binds a farnesyl group to the terminal cysteine residue, and releases its pyrophosphate (PP) group (13). FTI-277 is a potent Ras CaaX domain peptidomimetic that competes with Ras for the FTase active site (89) (Fig. 1).

Ras, FPP, and protein farnesylation have been examined to a limited degree in asthma (19, 65). Ras plays a role in IL-5–induced eosinophil transmigration when examined in vitro (90). Experiments using a dominant negative HIV-TAT Ras construct showed that Ras was necessary for the induction of the Th2 allergic response in mice (19).

In our study, treatment with FTI-277 in vivo had no significant effects on Ras cytosolic and membrane subcellular distribution in either FA or OVA exposure groups or on total Ras protein expression in whole-lung tissue homogenate (Fig. 2). Similarly, Ras GTPase activity was also not affected by drug treatment (Fig. 3). Despite these findings, treatment with FTI-277 exacerbated allergic inflammation (Fig. 4) and worsened lung function in mice (Fig. 7), indicating that it did have a significant yet negative pharmacologic effect in our mouse model.

The FTI-277 dose administered in mice was sufficiently high enough to inhibit FTase and subsequent Ras farnesylation. Based on our dosing regimen (see *Materials and Methods*), mice received the equivalent of 6.3 mM of FTI-277 per day, which is not only six orders of magnitude higher than the drug's IC_{50} of 50 nM, but it is three orders of magnitude higher than the drug concentrations used in our cell culture experiments (10 and 20 μM, Fig. 10). Therefore, either measuring Ras (and its GTPase activity) in whole-lung homogenate does not provide enough detail or granularity to detect such small changes in signaling, or the adverse effect of FTI-277 treatment in our model occurs by a different mechanism.

Effects of FPP and FTI-277 treatment in HBE1 cells

Using HBE1 cells in vitro, FPP augmented IL-13–induced STAT6 activation and eotaxin-3 secretion (Fig. 10A, 10C), but the lack of any significant differences in Ras cytosol and membrane content between IL-13 and IL-13 plus FPP (Fig. 10D) suggests a Ras-independent mechanism (Fig. 11). Although it is reasonable to think that the observed FPP effect likely involves Ras-independent farnesylation of proteins that then promote IL-13/STAT6 signaling (Fig. 11A), there may be other important effects of FPP not yet elucidated in bronchial epithelial cells involving Rab GTPase, cholesterol, or phosphoantigen signaling (Fig. 11B, 11D).

There are several plausible explanations for the lack of significant differences in Ras farnesylation between the IL-13 versus IL-13 plus FTI groups. One possibility is insufficient FTI-277 inhibition of FTase, which is tantamount to no inhibition of Ras farnesylation. However, this is highly unlikely given the high treatment concentrations used (10 and 20 μM) relative to the known IC_{50} of the drug (50 nM). We confirmed pharmacologic inhibition of Ras farnesylation by showing that FTI-277 significantly decreased the ratio of membrane-bound Ras while increasing cytosolic unprenylated Ras in epithelial cells (Figs. 1, 9).

However, treatment durations over a 72 h timeframe or longer (as in our mouse experiments), could lead to an increase in the intracellular pool of available FPP, which when metabolized to GGPP (Fig. 1) can lead to Ras geranylgeranylation (91). This would in turn result in increased membrane anchoring of geranylgeranylated Ras and increased Ras activation despite FTI-277 treatment. Biochemically speaking, it is possible that as the levels of farnesylated Ras declined due to FTI-277 treatment, geranylgeranylated Ras increased to yield a net of no significant change in membrane and cytosolic Ras (Fig. 10E). This mechanism could also explain the paradoxical enrichment of Ras membrane anchoring post FTI-227 treatment (control versus FTI, Fig. 10E). Whereas at shorter FTI-277 treatment durations (i.e., 30 min, Fig. 9A), this potential alternative geranylgeranylation does not seem to occur.

There are at least four other explanations for the lack of FTI-277 treatment effect. First, despite the fact that FTI-277 doses used in all of our animal and cell culture experiments far exceeded the drug's IC_{50} for FTase, it is possible that FTase inhibition of Ras farnesylation was not sufficient to block signaling of all three Ras isoforms (K-, H-, and N-Ras) (14, 79, 92, 93), resulting in residual Ras membrane tethering and continued Ras activity. Second, in addition to the known Ras posttranslational modifications of farnesylation and geranylgeranylation that facilitate membrane anchoring, Ras can also undergo palmitoylation (94). Our experiments did not assess for palmitoylation; therefore, this could also potentially explain persistent Ras activation despite FTase inhibition with FTI-277. Third, Ras GTPase can also undergo phosphorylation by kinases, which also controls its activity (80). And fourth, having confirmed the FTI-277 dose range (10–20 μM, Fig. 9A) that inhibits FTase at the shorter 30 min time point, we speculate that it is possible that the drug was metabolized, or compensatory mechanisms became active by 72 h such that FTase was no longer effectively inhibited.

The diverse roles and effects of FPP

FPP plays important roles in cellular biochemistry and physiology, and airway function is no exception. FPP is used both for farnesylation, which is necessary for the incorporation of small GTPases, such as Ras into cell membranes and as the precursor molecule for GGPP and cholesterol. In an ex vivo model of asthma, the addition of FPP or GGPP enhanced LPS-induced bronchoconstriction of isolated human bronchi (58), a mechanism relevant to human asthma pathogenesis.

Our results show that FPP exacerbates mucosal IL-13–mediated chemokine production in line with type 2 inflammatory responses in the airways. This is an important and novel observation that will require further study. There are several potential explanations for the synergistic effect of IL-13 plus FPP on eotaxin-3 peptide

secretion (Fig. 10A). The isoprenoid FPP has diverse biological roles in different disease models. In addition to its well-known role in Ras and protein farnesylation (13, 64), FPP can be metabolized into different effector molecules and also has direct effects on cells. In the MA pathway, which is fundamentally an anabolic cascade, FPP is metabolized to GGPP and further downstream to squalene then cholesterol (Fig. 1), both of which can activate immune cells leading to inflammation (59). These are critical molecules not only for the formation of cell membranes via cholesterol and small GTPase function for signal transduction but also oxysterol metabolism and the regulation of various transcription factors important in lipid biology and inflammation (95, 96), including the glucocorticoid receptor (GR) (66, 82, 97).

Like squalene synthase inhibitors (Fig. 1), the FTIs can theoretically increase inflammation by increasing the pool of unused endogenous FPP, which can farnesylate and activate GTPases in excess (66). FPP itself could lead to increased farnesylation of other non-Ras small GTPases (79, 98), such as Rho family GTPases like RhoB (99–101), farnesylation of non-GTPase proteins or kinases (81), and shunting of FPP to GGPP, resulting in increased geranylgeranylation of Rho and/or Rab family GTPases (Fig. 11B). For example, the antibiotic and FTI manumycin competes with FPP as a substrate for the FTase enzyme. In doing so, it increases FPP concentrations locally, and this can activate various transcription factors important in cell proliferation and inflammation (97).

In support of this idea, when we added FPP to IL-13, we observed enhanced STAT6 phosphorylation in HBE1 cells (Fig. 10C). Although we have not investigated the mechanism underlying this novel observation, it may involve farnesylation of a protein (or group of proteins) involved in the IL-13/STAT6/eotaxin cascade and/or due to direct FPP effects on epithelial cells. Fig. 11 summarizes some hypothetical mechanisms that we propose involving FPP and potential cellular responses relevant to airway epithelial type 2 inflammation.

Phosphoantigen biology and asthma

Isopentenyl pyrophosphate (IPP), an isoprenoid metabolite just upstream of FPP (Fig. 1), is the originally described phosphoantigen (102–104). Extracellular IPP is detected by γδ T cells via the butyrophilin receptor family as part of their immune surveillance program against infection (103) and malignant transformation (105–110).

Relevant to our work, γδ T cells have also been recognized to play a role in asthma pathogenesis (111). Given our results, is it possible that FPP could also function as a phosphoantigen (Fig. 11D)? At least with respect to activating γδ T cells, there is evidence to suggest that FPP (and GGPP) may function as phosphoantigens or have phosphoantigen-like properties but may be less potent than IPP (112). Whether this also happens in airway epithelial cells remains unknown.

It is intriguing to speculate whether phosphoantigens also play a role in asthma as a danger signal released by dying or diseased epithelial (or other types of) cells (Fig. 11D). This may be an important mechanism to study if FPP causes a significant elevation in the intensity of Th2 inflammation in human asthma, specifically IL-13–mediated signaling in the intact epithelial compartment. In a more general sense, phosphoantigen biology could be an important area to explore in the pathogenesis of asthma and other pulmonary diseases. Functionally speaking, FPP also leads to bronchoconstriction in isolated human airways (58), a response relevant to asthma and lung physiology. The therapeutic implications of this idea would be the development of novel therapies such as butyrophilin receptor antagonists or inhaled statins (113–116) and/or inhaled BPs (65), both of which deplete the pool of available FPP and GGPP, thus reducing the burden of isoprenoid phosphoantigens in the airways.

In conclusion, our prior work collectively indicates that depletion of MA pathway metabolites may be a useful therapeutic strategy in asthma and allergic inflammation. This current study suggests that inhibition of Ras farnesylation may not underlie the previously reported beneficial statin effects in asthma. Further, we have now shown that specific pharmacologic inhibition of FTase in allergic asthma in vivo, which blocks Ras farnesylation, may be harmful. However, Ras-independent protein farnesylation or direct cellular effects of FPP may contribute to airway epithelial Th2 cytokine production.

Beyond the statins alone, further research should continue to investigate the modulation of airway isoprenylation and the role of FPP in asthma pathogenesis. Based on our prior statin work, the results of this study, and recent publications assessing the role of FPPS, a therapeutic approach using FPPS inhibitors (such as BPs) and/or HMGCR inhibitors (such as statins) might yield better results. Therefore, inhibition of the production or release of cellular FPP might be a better therapeutic strategy than FTase or Ras inhibition in asthma.

Acknowledgments

We thank Keisha Williams, Simon Vu, and Kenneth Chmiel for technical assistance and input.

Disclosures

The authors have no financial conflicts of interest.

References

1. World Health Organization. 2007. *Global Surveillance, Prevention, and Control of Chronic Respiratory Diseases: A Comprehensive Approach.* World Health Organization, Geneva, Switzerland.
2. Yeganeh, B., E. Wiechec, S. R. Ande, P. Sharma, A. R. Moghadam, M. Post, D. H. Freed, M. Hashemi, S. Shojaei, A. A. Zeki, and S. Ghavami. 2014. Targeting the mevalonate cascade as a new therapeutic approach in heart disease, cancer and pulmonary disease. *Pharmacol. Ther.* 143: 87–110.
3. Chiba, Y., S. Sato, and M. Misawa. 2008. Inhibition of antigen-induced bronchial smooth muscle hyperresponsiveness by lovastatin in mice. *J. Smooth Muscle Res.* 44: 123–128.
4. Huang, C.-F., H.-J. Peng, C.-C. Wu, W.-T. Lo, Y.-L. Shih, and T.-C. Wu. 2013. Effect of oral administration with pravastatin and atorvastatin on airway hyperresponsiveness and allergic reactions in asthmatic mice. *Ann. Allergy Asthma Immunol.* 110: 11–17.
5. Ahmad, T., U. Mabalirajan, A. Sharma, J. Aich, L. Makhija, B. Ghosh, and A. Agrawal. 2011. Simvastatin improves epithelial dysfunction and airway hyperresponsiveness: from asymmetric dimethyl-arginine to asthma. *Am. J. Respir. Cell Mol. Biol.* 44: 531–539.
6. Zeki, A. A., L. Franzi, J. Last, and N. J. Kenyon. 2009. Simvastatin inhibits airway hyperreactivity: implications for the mevalonate pathway and beyond. *Am. J. Respir. Crit. Care Med.* 180: 731–740.
7. Zeki, A. A., J. M. Bratt, M. Rabowsky, J. A. Last, and N. J. Kenyon. 2010. Simvastatin inhibits goblet cell hyperplasia and lung arginase in a mouse model of allergic asthma: a novel treatment for airway remodeling? *Transl. Res.* 156: 335–349.
8. Liao, J. K., and U. Laufs. 2005. Pleiotropic effects of statins. *Annu. Rev. Pharmacol. Toxicol.* 45: 89–118.
9. Wang, C.-Y., P.-Y. Liu, and J. K. Liao. 2008. Pleiotropic effects of statin therapy: molecular mechanisms and clinical results. *Trends Mol. Med.* 14: 37–44.
10. Roy, A., M. Jana, M. Kundu, G. T. Corbett, S. B. Rangaswamy, R. K. Mishra, C. H. Luan, F. J. Gonzalez, and K. Pahan. 2015. HMG-CoA reductase inhibitors bind to PPARα to upregulate neurotrophin expression in the brain and improve memory in mice. *Cell Metab.* 22: 253–265.
11. Sandhu, K., S. Ott, R. Wu, and A. A. Zeki. 2014. The mevalonate pathway regulates eotaxin-3 secretion from human airway epithelial cells: a therapeutic role for simvastatin in asthma. *J. Invest. Med.* 62: 197–198.
12. McTaggart, S. J. 2006. Isoprenylated proteins. *Cell. Mol. Life Sci.* 63: 255–267.
13. Greenwood, J., L. Steinman, and S. S. Zamvil. 2006. Statin therapy and autoimmune disease: from protein prenylation to immunomodulation. *Nat. Rev. Immunol.* 6: 358–370.
14. Schmick, M., A. Kraemer, and P. I. Bastiaens. 2015. Ras moves to stay in place. *Trends Cell Biol.* 25: 190–197.
15. Goto, K., Y. Chiba, K. Matsusue, Y. Hattori, Y. Maitani, H. Sakai, S. Kimura, and M. Misawa. 2010. The proximal STAT6 and NF-kappaB sites are responsible for IL-13- and TNF-alpha-induced RhoA transcriptions in human bronchial smooth muscle cells. *Pharmacol. Res.* 61: 466–472.

16. Chiba, Y., J. Arima, H. Sakai, and M. Misawa. 2008. Lovastatin inhibits bronchial hyperresponsiveness by reducing RhoA signaling in rat allergic asthma. *Am. J. Physiol. Lung Cell. Mol. Physiol.* 294: L705–L713.
17. Schaafsma, D., S. S. Roscioni, H. Meurs, and M. Schmidt. 2008. Monomeric G-proteins as signal transducers in airway physiology and pathophysiology. *Cell. Signal.* 20: 1705–1714.
18. Chiba, Y., S. Sato, and M. Misawa. 2009. GGTI-2133, an inhibitor of geranylgeranyltransferase, inhibits infiltration of inflammatory cells into airways in mouse experimental asthma. *Int. J. Immunopathol. Pharmacol.* 22: 929–935.
19. Myou, S., X. Zhu, S. Myo, E. Boetticher, A. Y. Meliton, J. Liu, N. M. Munoz, and A. R. Leff. 2003. Blockade of airway inflammation and hyperresponsiveness by HIV-TAT-dominant negative Ras. *J. Immunol.* 171: 4379–4384.
20. Luo, F. 2004. Simvastatin induces eosinophil apoptosis in vitro. *Chest* 126: 721S.
21. Hall, D. J., J. Cui, M. E. Bates, B. A. Stout, L. Koenderman, P. J. Coffer, and P. J. Bertics. 2001. Transduction of a dominant-negative H-Ras into human eosinophils attenuates extracellular signal-regulated kinase activation and interleukin-5-mediated cell viability. *Blood* 98: 2014–2021.
22. Zhu, Y., and P. J. Bertics. 2011. Chemoattractant-induced signaling via the Ras-ERK and PI3K-Akt networks, along with leukotriene C4 release, is dependent on the tyrosine kinase Lyn in IL-5- and IL-3-primed human blood eosinophils. *J. Immunol.* 186: 516–526.
23. Shibata, Y., T. Kamata, M. Kimura, M. Yamashita, C. R. Wang, K. Murata, M. Miyazaki, M. Taniguchi, N. Watanabe, and T. Nakayama. 2002. Ras activation in T cells determines the development of antigen-induced airway hyperresponsiveness and eosinophilic inflammation. *J. Immunol.* 169: 2134–2140.
24. McKay, A., B. P. Leung, I. B. McInnes, N. C. Thomson, and F. Y. Liew. 2004. A novel anti-inflammatory role of simvastatin in a murine model of allergic asthma. *J. Immunol.* 172: 2903–2908.
25. Kim, D. Y., S. Y. Ryu, J. E. Lim, Y. S. Lee, and J. Y. Ro. 2007. Anti-inflammatory mechanism of simvastatin in mouse allergic asthma model. *Eur. J. Pharmacol.* 557: 76–86.
26. Choy, D. F., B. Modrek, A. R. Abbas, S. Kummerfeld, H. F. Clark, L. C. Wu, G. Fedorowicz, Z. Modrusan, J. V. Fahy, P. G. Woodruff, and J. R. Arron. 2011. Gene expression patterns of Th2 inflammation and intercellular communication in asthmatic airways. *J. Immunol.* 186: 1861–1869.
27. Coleman, J. M., C. Naik, F. Holguin, A. Ray, P. Ray, J. B. Trudeau, and S. E. Wenzel. 2012. Epithelial eotaxin-2 and eotaxin-3 expression: relation to asthma severity, luminal eosinophilia and age at onset. *Thorax* 67: 1061–1066.
28. Kenyon, N. J., K. Gohil, and J. A. Last. 2003. Susceptibility to ovalbumin-induced airway inflammation and fibrosis in inducible nitric oxide synthetase-deficient mice: mechanisms and consequences. *Toxicol. Appl. Pharmacol.* 191: 2–11.
29. Kenyon, N. J., R. W. Ward, and J. A. Last. 2003. Airway fibrosis in a mouse model of airway inflammation. *Toxicol. Appl. Pharmacol.* 186: 90–100.
30. Kenyon, N. J., and J. A. Last. 2005. Reversible and irreversible airway inflammation and fibrosis in mice exposed to inhaled ovalbumin. *Inflamm. Res.* 54: 57–65.
31. Robinson, C. B., and R. Wu. 1991. Culture of conducting airway epithelial in serum-free medium. *J. Tissue Cult. Methods* 13: 95–102.
32. Wu, R., E. Nolan, and C. Turner. 1985. Expression of tracheal differentiated functions in serum-free hormone-supplemented medium. *J. Cell. Physiol.* 125: 167–181.
33. Whitcutt, M. J., K. B. Adler, and R. Wu. 1988. A biphasic chamber system for maintaining polarity of differentiation of cultured respiratory tract epithelial cells. *In Vitro Cell. Dev. Biol.* 24: 420–428.
34. Statt, S., J.-W. Ruan, L.-Y. Hung, C. Y. Chang, C. T. Huang, J. H. Lim, J. D. Li, R. Wu, and C. Y. Kao. 2015. Statin-conferred enhanced cellular resistance against bacterial pore-forming toxins in airway epithelial cells. *Am. J. Respir. Cell Mol. Biol.* 53: 689–702.
35. Yankaskas, J. R., J. E. Haizlip, M. Conrad, D. Koval, E. Lazarowski, A. M. Paradiso, C. A. Rinehart, Jr., B. Sarkadi, R. Schlegel, and R. C. Boucher. 1993. Papilloma virus immortalized tracheal epithelial cells retain a well-differentiated phenotype. *Am. J. Physiol.* 264: C1219–C1230.
36. Gibbs, J. B., S. L. Graham, G. D. Hartman, K. S. Koblan, N. E. Kohl, C. A. Omer, and A. Oliff. 1997. Farnesyltransferase inhibitors versus Ras inhibitors. *Curr. Opin. Chem. Biol.* 1: 197–203.
37. Efuet, E. T., and K. Keyomarsi. 2006. Farnesyl and geranylgeranyl transferase inhibitors induce G1 arrest by targeting the proteasome. *Cancer Res.* 66: 1040–1051.
38. So, E.-Y., J. Oh, J.-Y. Jang, J.-H. Kim, and C.-E. Lee. 2007. Ras/Erk pathway positively regulates Jak1/STAT6 activity and IL-4 gene expression in Jurkat T cells. *Mol. Immunol.* 44: 3416–3426.
39. Hesterberg, T. W., J. E. Gerriets, K. M. Reiser, A. C. Jackson, C. E. Cross, and J. A. Last. 1981. Bleomycin-induced pulmonary fibrosis: correlation of biochemical, physiological, and histological changes. *Toxicol. Appl. Pharmacol.* 60: 360–367.
40. Holgate, S. T. 2007. Epithelium dysfunction in asthma. *J. Allergy Clin. Immunol.* 120: 1233–1244; quiz 1245–1246.
41. Holgate, S. T. 2008. The airway epithelium is central to the pathogenesis of asthma. *Allergol. Int.* 57: 1–10.
42. Leino, M.S., M. Loxham, C. Blume, E.J. Swindle, N.P Jayasekera, P. W. Dennison, B.W. Shamji, M.J. Edwards, S.T. Holgate, P.H. Howarth, and D. E. Davies. 2013. Barrier disrupting effects of alternaria alternata extract on bronchial epithelium from asthmatic donors. *PLoS One* 8: e71278.
43. Zeki, A. A., P. Thai, N. J. Kenyon, and R. Wu. 2012. Differential effects of simvastatin on IL-13-induced cytokine gene expression in primary mouse tracheal epithelial cells. *Respir. Res.* 13: 38–46.
44. Dunn, S. E., S. Youssef, M. J. Goldstein, T. Prod'homme, M. S. Weber, S. S. Zamvil, and L. Steinman. 2006. Isoprenoids determine Th1/Th2 fate in pathogenic T cells, providing a mechanism of modulation of autoimmunity by atorvastatin. *J. Exp. Med.* 203: 401–412.
45. Chung, K. F. 2015. Targeting the interleukin pathway in the treatment of asthma. *Lancet* 386: 1086–1096.
46. Munitz, A., E. B. Brandt, M. Mingler, F. D. Finkelman, and M. E. Rothenberg. 2008. Distinct roles for IL-13 and IL-4 via IL-13 receptor alpha1 and the type II IL-4 receptor in asthma pathogenesis. *Proc. Natl. Acad. Sci. USA* 105: 7240–7245.
47. Hebenstreit, D., G. Wirnsberger, J. Horejs-Hoeck, and A. Duschl. 2006. Signaling mechanisms, interaction partners, and target genes of STAT6. *Cytokine Growth Factor Rev.* 17: 173–188.
48. Peng, Q., T. Matsuda, and S. J. Hirst. 2004. Signaling pathways regulating interleukin-13-stimulated chemokine release from airway smooth muscle. *Am. J. Respir. Crit. Care Med.* 169: 596–603.
49. Thai, P., Y. Chen, G. Dolganov, and R. Wu. 2005. Differential regulation of MUC5AC/Muc5ac and hCLCA-1/mGob-5 expression in airway epithelium. *Am. J. Respir. Cell Mol. Biol.* 33: 523–530.
50. Li, L., Y. Xia, A. Nguyen, Y. H. Lai, L. Feng, T. R. Mosmann, and D. Lo. 1999. Effects of Th2 cytokines on chemokine expression in the lung: IL-13 potently induces eotaxin expression by airway epithelial cells. *J. Immunol.* 162: 2477–2487.
51. Hirst, S. J., M. P. Hallsworth, Q. Peng, and T. H. Lee. 2002. Selective induction of eotaxin release by interleukin-13 or interleukin-4 in human airway smooth muscle cells is synergistic with interleukin-1beta and is mediated by the interleukin-4 receptor alpha-chain. *Am. J. Respir. Crit. Care Med.* 165: 1161–1171.
52. Lilly, C. M., H. Nakamura, H. Kesselman, C. Nagler-Anderson, K. Asano, E. A. Garcia-Zepeda, M. E. Rothenberg, J. M. Drazen, and A. D. Luster. 1997. Expression of eotaxin by human lung epithelial cells: induction by cytokines and inhibition by glucocorticoids. *J. Clin. Invest.* 99: 1767–1773.
53. Ravensberg, A. J., F. L. Ricciardolo, A. van Schadewijk, K. F. Rabe, P. J. Sterk, P. S. Hiemstra, and T. Mauad. 2005. Eotaxin-2 and eotaxin-3 expression is associated with persistent eosinophilic bronchial inflammation in patients with asthma after allergen challenge. *J. Allergy Clin. Immunol.* 115: 779–785.
54. Komiya, A., H. Nagase, H. Yamada, T. Sekiya, M. Yamaguchi, Y. Sano, N. Hanai, A. Furuya, K. Ohta, K. Matsushima, et al. 2003. Concerted expression of eotaxin-1, eotaxin-2, and eotaxin-3 in human bronchial epithelial cells. *Cell. Immunol.* 225: 91–100.
55. Larose, M. C., J. Chakir, A. S. Archambault, P. Joubert, V. Provost, M. Laviolette, and N. Flamand. 2015. Correlation between CCL26 production by human bronchial epithelial cells and airway eosinophils: involvement in patients with severe eosinophilic asthma. *J. Allergy Clin. Immunol.* 136: 904–913.
56. Woodruff, P. G., H. A. Boushey, G. M. Dolganov, C. S. Barker, Y. H. Yang, S. Donnelly, A. Ellwanger, S. S. Sidhu, T. P. Dao-Pick, C. Pantoja, et al. 2007. Genome-wide profiling identifies epithelial cell genes associated with asthma and with treatment response to corticosteroids. *Proc. Natl. Acad. Sci. USA* 104: 15858–15863.
57. Woodruff, P. G., B. Modrek, D. F. Choy, G. Jia, A. R. Abbas, A. Ellwanger, L. L. Koth, J. R. Arron, and J. V. Fahy. 2009. T-helper type 2-driven inflammation defines major subphenotypes of asthma. *Am. J. Respir. Crit. Care Med.* 180: 388–395.
58. Cazzola, M., L. Calzetta, C. P. Page, B. Rinaldi, A. Capuano, and M. G. Matera. 2011. Protein prenylation contributes to the effects of LPS on EFS-induced responses in human isolated bronchi. *Am. J. Respir. Cell Mol. Biol.* 45: 704–710.
59. Fessler, M. B. 2015. Regulation of adaptive immunity in health and disease by cholesterol metabolism. *Curr. Allergy Asthma Rep.* 15: 48.
60. Thurnher, M., and G. Gruenbacher. 2015. T lymphocyte regulation by mevalonate metabolism. *Sci. Signal.* 8: re4.
61. Chiba, Y., S. Sato, and M. Misawa. 2009. Lovastatin inhibits antigen-induced airway eosinophilia without affecting the production of inflammatory mediators in mice. *Inflamm. Res.* 58: 363–369.
62. Scheele, J. S., R. E. Marks, and G. R. Boss. 2007. Signaling by small GTPases in the immune system. *Immunol. Rev.* 218: 92–101.
63. Popoff, M. R., and B. Geny. 2009. Multifaceted role of Rho, Rac, Cdc42 and Ras in intercellular junctions, lessons from toxins. *Biochim. Biophys. Acta* 1788: 797–812.
64. Downward, J. 2003. Targeting RAS signalling pathways in cancer therapy. *Nat. Rev. Cancer* 3: 11–22.
65. Sasaki, O., M. Imamura, Y. Yamazumi, H. Harada, T. Matsumoto, K. Okunishi, K. Nakagome, R. Tanaka, T. Akiyama, K. Yamamoto, and M. Dohi. 2013. Alendronate attenuates eosinophilic airway inflammation associated with suppression of Th2 cytokines, Th17 cytokines, and eotaxin-2. *J. Immunol.* 191: 2879–2889.
66. Das, S., M. Schapira, M. Tomic-Canic, R. Goyanka, T. Cardozo, and H. H. Samuels. 2007. Farnesyl pyrophosphate is a novel transcriptional activator for a subset of nuclear hormone receptors. *Mol. Endocrinol.* 21: 2672–2686.
67. Maltese, W. A., G. Soule, W. Gunning, E. Calomeni, and B. Alexander. 2002. Mutant Rab24 GTPase is targeted to nuclear inclusions. *BMC Cell Biol.* 3: 25.
68. Stenmark, H. 2009. Rab GTPases as coordinators of vesicle traffic. *Nat. Rev. Mol. Cell Biol.* 10: 513–525.
69. Bhuin, T., and J. K. Roy. 2014. Rab proteins: the key regulators of intracellular vesicle transport. *Exp. Cell Res.* 328: 1–19.

70. Hutagalung, A. H., and P. J. Novick. 2011. Role of Rab GTPases in membrane traffic and cell physiology. *Physiol. Rev.* 91: 119–149.
71. Leung, K. F., R. Baron, and M. C. Seabra. 2006. Thematic review series: lipid posttranslational modifications. geranylgeranylation of Rab GTPases. *J. Lipid Res.* 47: 467–475.
72. Hakamada-Taguchi, R., Y. Uehara, K. Kuribayashi, A. Numabe, K. Saito, H. Negoro, T. Fujita, T. Toyo-oka, and T. Kato. 2003. Inhibition of hydroxymethylglutaryl-coenzyme a reductase reduces Th1 development and promotes Th2 development. *Circ. Res.* 93: 948–956.
73. Waiczies, S., I. Bendix, and F. Zipp. 2008. Geranylgeranylation but not GTP-loading of Rho GTPases determines T cell function. *Sci. Signal.* 1: pt3.
74. Ghittoni, R., L. Patrussi, K. Pirozzi, M. Pellegrini, P. E. Lazzerini, P. L. Capecchi, F. L. Pasini, and C. T. Baldari. 2005. Simvastatin inhibits T-cell activation by selectively impairing the function of Ras superfamily GTPases. *FASEB J.* 19: 605–607.
75. Imamura, M., K. Okunishi, H. Ohtsu, K. Nakagome, H. Harada, R. Tanaka, K. Yamamoto, and M. Dohi. 2009. Pravastatin attenuates allergic airway inflammation by suppressing antigen sensitisation, interleukin 17 production and antigen presentation in the lung. *Thorax* 64: 44–49.
76. Xue, X., K. T. Lai, J. F. Huang, Y. Gu, L. Karlsson, and A. Fourie. 2006. Anti-inflammatory activity in vitro and in vivo of the protein farnesyltransferase inhibitor tipifarnib. *J. Pharmacol. Exp. Ther.* 317: 53–60.
77. Albeck, J. G., G. B. Mills, and J. S. Brugge. 2013. Frequency-modulated pulses of ERK activity transmit quantitative proliferation signals. *Mol. Cell* 49: 249–261.
78. Agudo-Ibáñez, L., A. Herrero, M. Barbacid, and P. Crespo. 2015. H-ras distribution and signaling in plasma membrane microdomains are regulated by acylation and deacylation events. *Mol. Cell. Biol.* 35: 1898–1914.
79. Papke, B., M. Schmick, N. Vartak, and P. I. H. Bastiaens. 2014. Chapter 8: the spatial organization of Ras signaling. In *Ras Superfamily Small G Proteins: Biology and Mechanisms I.* Springer, Berlin, p.173–188.
80. Bunda, S., P. Heir, T. Srikumar, J. D. Cook, K. Burrell, Y. Kano, J. E. Lee, G. Zadeh, B. Raught, and M. Ohh. 2014. Src promotes GTPase activity of Ras via tyrosine 32 phosphorylation. *Proc. Natl. Acad. Sci. USA* 111: E3785–E3794.
81. Charron, G., M. M. H. Li, M. R. MacDonald, and H. C. Hang. 2013. Prenylome profiling reveals S-farnesylation is crucial for membrane targeting and antiviral activity of ZAP long-isoform. *Proc. Natl. Acad. Sci. USA* 110: 11085–11090.
82. Vukelic, S., O. Stojadinovic, I. Pastar, C. Vouthounis, A. Krzyzanowska, S. Das, H. H. Samuels, and M. Tomic-Canic. 2010. Farnesyl pyrophosphate inhibits epithelialization and wound healing through the glucocorticoid receptor. *J. Biol. Chem.* 285: 1980–1988.
83. Lerner, E. C., Y. Qian, M. A. Blaskovich, R. D. Fossum, A. Vogt, J. Sun, A. D. Cox, C. J. Der, A. D. Hamilton, and S. M. Sebti. 1995. Ras CAAX peptidomimetic FTI-277 selectively blocks oncogenic Ras signaling by inducing cytoplasmic accumulation of inactive Ras-Raf complexes. *J. Biol. Chem.* 270: 26802–26806.
84. Lerner, E. C., T. T. Zhang, D. B. Knowles, Y. Qian, A. D. Hamilton, and S. M. Sebti. 1997. Inhibition of the prenylation of K-Ras, but not H- or N-Ras, is highly resistant to CAAX peptidomimetics and requires both a farnesyltransferase and a geranylgeranyltransferase I inhibitor in human tumor cell lines. *Oncogene* 15: 1283–1288.
85. Pelaia, G., L. Gallelli, T. Renda, D. Fratto, D. Falcone, M. Caraglia, M. T. Busceti, R. Terracciano, A. Vatrella, R. Maselli, and R. Savino. 2012. Effects of statins and farnesyl transferase inhibitors on ERK phosphorylation, apoptosis and cell viability in non-small lung cancer cells. *Cell Prolif.* 45: 557–565.
86. Sebti, S. M., and A. D. Hamilton. 2000. Farnesyltransferase and geranylgeranyltransferase I inhibitors and cancer therapy: lessons from mechanism and bench-to-bedside translational studies. *Oncogene* 19: 6584–6593.
87. Cox, A. D., and C. J. Der. 2002. Farnesyltransferase inhibitors: promises and realities. *Curr. Opin. Pharmacol.* 2: 388–393.
88. Lobell, R. B., C. A. Omer, M. T. Abrams, H. G. Bhimnathwala, M. J. Brucker, C. A. Buser, J. P. Davide, S. J. deSolms, C. J. Dinsmore, M. S. Ellis-Hutchings, et al. 2001. Evaluation of farnesyl:protein transferase and geranylgeranyl:protein transferase inhibitor combinations in preclinical models. *Cancer Res.* 61: 8758–8768.
89. Lee, K. H., M. Koh, and A. Moon. 2016. Farnesyl transferase inhibitor FTI-277 inhibits breast cell invasion and migration by blocking H-Ras activation. *Oncol. Lett.* 12: 2222–2226.
90. Bates, M. E., J. B. Sedgwick, Y. Zhu, L. Y. Liu, R. G. Heuser, N. N. Jarjour, H. Kita, and P. J. Bertics. 2010. Human airway eosinophils respond to chemoattractants with greater eosinophil-derived neurotoxin release, adherence to fibronectin, and activation of the Ras-ERK pathway when compared with blood eosinophils. *J. Immunol.* 184: 7125–7133.
91. Whyte, D. B., P. Kirschmeier, T. N. Hockenberry, I. Nunez-Oliva, L. James, J. J. Catino, W. R. Bishop, and J. K. Pai. 1997. K- and N-Ras are geranylgeranylated in cells treated with farnesyl protein transferase inhibitors. *J. Biol. Chem.* 272: 14459–14464.
92. Basso, A. D., P. Kirschmeier, and W. R. Bishop. 2006. Lipid posttranslational modifications. Farnesyl transferase inhibitors. *J. Lipid Res.* 47: 15–31.
93. Omerovic, J., and I. A. Prior. 2009. Compartmentalized signalling: Ras proteins and signalling nanoclusters. *FEBS J.* 276: 1817–1825.
94. Aicart-Ramos, C., R.A. Valero, and I. Rodriguez-Crespo. 2011. Protein palmitoylation and subcellular trafficking. *Biochim. Biophys. Acta Biomembr.* 1808: 2981–2994.
95. Koarai, A., S. Yanagisawa, H. Sugiura, T. Ichikawa, T. Kikuchi, K. Furukawa, K. Akamatsu, T. Hirano, M. Nakanishi, K. Matsunaga, et al. 2012. 25-Hydroxycholesterol enhances cytokine release and Toll-like receptor 3 response in airway epithelial cells. *Respir. Res.* 13: 63.
96. Rezen, T., D. Rozman, J. M. Pascussi, and K. Monostory. 2011. Interplay between cholesterol and drug metabolism. *Biochim. Biophys. Acta.* 1814: 146–160.
97. Zhuravliova, E., T. Barbakadze, N. Narmania, J. Ramsden, and D. Mikeladze. 2007. Inhibition of nitric oxide synthase and farnesyltransferase change the activities of several transcription factors. *J. Mol. Neurosci.* 31: 281–287.
98. Roberts, P. J., N. Mitin, P. J. Keller, E. J. Chenette, J. P. Madigan, R. O. Currin, A. D. Cox, O. Wilson, P. Kirschmeier, and C. J. Der. 2008. Rho Family GTPase modification and dependence on CAAX motif-signaled posttranslational modification. *J. Biol. Chem.* 283: 25150–25163.
99. Wang, X. H., Y. Wang, F. Diao, and J. Lu. 2013. RhoB is involved in lipopolysaccharide-induced inflammation in mouse in vivo and in vitro. *J. Physiol. Biochem.* 69: 189–197.
100. Luis-Ravelo, D., I. Antón, C. Zandueta, K. Valencia, M. J. Pajares, J. Agorreta, L. Montuenga, S. Vicent, I. I. Wistuba, J. De Las Rivas, and F. Lecanda. 2014. RHOB influences lung adenocarcinoma metastasis and resistance in a host-sensitive manner. *Mol. Oncol.* 8: 196–206.
101. Wojciak-Stothard, B., L. Zhao, E. Oliver, O. Dubois, Y. Wu, D. Kardassis, E. Vasilaki, M. Huang, J. A. Mitchell, L. S. Harrington, et al. 2012. Role of RhoB in the regulation of pulmonary endothelial and smooth muscle cell responses to hypoxia. [Published erratum appears in 2012 *Circ. Res.* 111: e163.] *Circ. Res.* 110: 1423–1434.
102. Li, J., M. J. Herold, B. Kimmel, I. Müller, B. Rincon-Orozco, V. Kunzmann, and T. Herrmann. 2009. Reduced expression of the mevalonate pathway enzyme farnesyl pyrophosphate synthase unveils recognition of tumor cells by Vgamma9Vdelta2 T cells. *J. Immunol.* 182: 8118–8124.
103. Spencer, C. T., G. Abate, A. Blazevic, and D. F. Hoft. 2008. Only a subset of phosphoantigen-responsive gamma9delta2 T cells mediate protective tuberculosis immunity. *J. Immunol.* 181: 4471–4484.
104. Dieli, F., R. Fadda, and N. Caccamo. 2014. Butyrophilin 3A1 presents phosphoantigens to human γδ T cells: the fourth model of antigen presentation in the immune system. *Cell. Mol. Immunol.* 11: 123–125.
105. Champagne, E. 2011. γδ T cell receptor ligands and modes of antigen recognition. *Arch. Immunol. Ther. Exp. (Warsz.)* 59: 117–137.
106. Kabelitz, D., and J. Dechanet-Merville. 2015. Editorial: "recent advances in gamma/delta T cell biology: new ligands, new functions, and new translational perspectives." *Front. Immunol.* 6: 371.
107. De Libero, G. 1997. Sentinel function of broadly reactive human gamma delta T cells. *Immunol. Today* 18: 22–26.
108. Karunakaran, M. M., and T. Herrmann. 2014. The Vγ9Vδ2 T cell antigen receptor and butyrophilin-3 A1: models of interaction, the possibility of co-evolution, and the case of dendritic epidermal T cells. *Front. Immunol.* 5: 648.
109. Rhodes, D. A., H.-C. Chen, A. J. Price, A. H. Keeble, M. S. Davey, L. C. James, M. Eberl, and J. Trowsdale. 2015. Activation of human γδ T cells by cytosolic interactions of BTN3A1 with soluble phosphoantigens and the cytoskeletal adaptor periplakin. *J. Immunol.* 194: 2390–2398.
110. De Libero, G., S.Y. Lau, and L. Mori. 2015. Phosphoantigen presentation to TCR γδ cells, a conundrum getting less gray zones. *Front. Immunol.* 5: 679.
111. Ullah, M. A., J. A. Revez, Z. Loh, J. Simpson, V. Zhang, L. Bain, A. Varelias, S. Rose-John, A. Blumenthal, M. J. Smyth, et al. 2015. Allergen-induced IL-6 trans-signaling activates γδ T cells to promote type 2 and type 17 airway inflammation. *J. Allergy Clin. Immunol.* 136: 1065–1073.
112. Morita, C. T., H. K. Lee, H. Wang, H. Li, R. A. Mariuzza, and Y. Tanaka. 2001. Structural features of nonpeptide prenyl pyrophosphates that determine their antigenicity for human gamma delta T cells. *J. Immunol.* 167: 36–41.
113. Zeki, A. A., J. M. Bratt, K. Y. Chang, L. M. Franzi, S. Ott, M. Silveria, O. Fiehn, J. A. Last, and N. J. Kenyon. 2015. Intratracheal instillation of pravastatin for the treatment of murine allergic asthma: a lung-targeted approach to deliver statins. *Physiol. Rep.* 3: e12352.
114. Xu, L., X. W. Dong, L. L. Shen, F. F. Li, J. X. Jiang, R. Cao, H. Y. Yao, H. J. Shen, Y. Sun, and Q. M. Xie. 2012. Simvastatin delivery via inhalation attenuates airway inflammation in a murine model of asthma. *Int. Immunopharmacol.* 12: 556–564.
115. Tulbah, A. S., H. X. Ong, P. Colombo, P. M. Young, and D. Traini. 2014. Novel simvastatin inhalation formulation and characterisation. *AAPS PharmSciTech* 15: 956–962.
116. Tulbah, A. S., H. X. Ong, L. Morgan, P. Colombo, P. M. Young, and D. Traini. 2015. Dry powder formulation of simvastatin. *Expert Opin. Drug Deliv.* 12: 857–868.